PROPOSAL

for

MEASUREMENT OF ELECTRON-DEUTERON ELASTIC AND INELASTIC MAGNETIC STRUCTURE FUNCTIONS AT LARGE MOMENTUM TRANSFER

by

R. G. Arnold, B. T. Chertok, S. Rock,
I. A. Schmidt, and Z. M. Szalata

The American University, Washington, D.C. 20016

and

B. A. Mecking

Universitat Bonn, Bonn, West Germany

Spokesperson: R. G. Arnold

THE AMERICAN UNIVERSITY
WASHINGTON, DISTRICT OF COLUMBIA 20016

College of Arts and Sciences
DEPARTMENT OF PHYSICS

February 16, 1978

Letter of Transmittal

To: Dr. G. Fischer, Secretary
Program Advisory Committee
SLAC

Dr. W.K.H. Panofsky, Director
SLAC

Members of the Program Advisory Committee

Dear Sirs:

The enclosed proposal is a request for 970 hours of five-sector electron beam in End Station A at 180 pps (75% efficiency included). We propose to build a new injector, called Injector East, at Sector 26 of the linac to produce an electron beam in the energy range of 0.4 to 2.9 GeV with 27 to 54 μA average current at 360 pps. This is as much as a factor of 10 to 20 increase in intensity over what is presently available at SLAC in that energy range. There does not now exist a comparable electron beam anywhere.

We propose to use this unique electron beam in our continuing investigation of the structure functions of light nuclei at large momentum transfer by the method of electron scattering. The proposed experiment, described in detail in this proposal, is to do elastic and inelastic electron scattering from the deuteron at backward ($\sim 155^{o}$) and forward ($\sim 40^{o}$) angles and to extract the magnetic structure functions $B(Q^2)$ and $2MW_1(Q^2,\nu)$ at large momentum transfer Q^2. This experiment will be a direct extension of our previous measurement of electron scattering from the deuteron at 8^{o} carried out at SLAC in 1974 (SLAC Experiment E101), and it will measure the magnetic structure functions to the maximum Q^2 attainable with the present generation of electron accelerators. The clean electromagnetic probe at high Q^2 will provide a powerful look at the details of the interaction of two nucleons at short distances. The new data will be an important guide to our understanding of such physics as: relativistic deuteron wave functions, isoscalar and isovector meson-exchange currents, and the role of quarks in the deuteron.

The enclosed proposal has been submitted to the National Science

Foundation and the Department of Energy as a request for funding for the major item of equipment, Injector East. For that reason the text is somewhat more detailed than may be customary for the usual SLAC proposal, as the NSF and DOE reviewers are not expected to be familiar with the facilities at SLAC. Also, since the subject of the experiment covers a range of topics in both nuclear and particle physics, we have included detailed discussions of the theoretical questions in both fields for the benefit of readers who may be familiar with one area but less so with the other.

We are aware that the new high intensity 0.4 to 2.9 GeV electron beam will significantly extend the capabilities of the SLAC linac as a research tool, and will open up the possibility for other uses besides this experiment. We have in mind future experiments, briefly described but not proposed in the following proposal, to measure the magnetic structure functions of ^{3}He and ^{3}H and large Q^2. They will also yield information about the interaction of nucleons at short distances. The physics questions to be explored are similar to those for the deuteron, with the additional possibility of learning about features of the nucleon-nucleon interaction present in the three-body system but not in the deuteron.

It is also possible that the new injector beam would be used to fill the SPEAR ring with electrons when SPEAR is running as a dedicated synchrotron radiation source after PEP turns on. (See the letter of support from the Director of the Stanford Synchrotron Radiation Laboratory attached below.)

The proposed injector has been designed, and will be constructed, installed, and tested by the SLAC staff over a period of approximately two years. Since this project requires two years lead time before physics experiments could begin, we are submitting the proposal for your approval at this early date. The time frame we suggest, pending approval of funding and approval by the Director of SLAC, is to begin construction as soon as possible, perhaps 1 May 1979. We will be completing the final stages of our approved experiment on electron-neutron scattering (SLAC Experiment E-133) by about January 1981, when we could commence activities on the new experiment proposed here. For your information, the correspondence with Dr. Panofsky beginning in August 1978, when this proposal was first submitted to SLAC, is enclosed below.

Finally, we note that the manpower listed on the title page are those people presently committed to the project. We will add other manpower during the actual data taking period to bring the total to approximately eight physicists.

Sincerely,

Raymond G. Arnold

Raymond G. Arnold
Spokesperson

RGA/wh
Enclosures

STANFORD UNIVERSITY

STANFORD LINEAR ACCELERATOR CENTER

Mail Address
SLAC, P. O. Box 4349
Stanford, California 94305

August 17, 1978

Dr. Raymond G. Arnold
Department of Physics
The American University
Washington, D. C. 20016

Dear Ray:

Thanks very much for your letter of August 4, 1978, asking a number of questions relating to the proposal entitled, "Measurement of Electron Deuteron Elastic and Inelastic Magnetic Structure Functions at Large Momentum Transfer," submitted by you and your colleagues. In this letter I will do my best to supply the answers.

We consider implementation of this proposal, if approved, to be a major modification of SLAC's facilities. Accordingly, the decision whether to go forward with this activity rests on the shoulders of the SLAC management in consultation with the Scientific Policy Committee. The reasons for considering the proposed added off-axis beam at Sector 26 to be a major modification are both its direct and implied cost, and also its program implications. Addition of this facility will provide a high intensity, low energy beam primarily for use in target area A but also for SSRL injection and possibly other uses in middle and low energy nuclear physics. Although the use of this new beam is compatible with most modes of operation of SLAC, it is not totally compatible with all of them. Specifically, SLAC cannot be operated in the SLED mode for its last 4 sectors when the proposed beam is in operation; this in turn lowers available electron beam energies for some experiments and also lowers the maximum positron injection energies into PEP during the time the proposed beam is in operation. Moreover, the installation of the proposed beam implies a commitment for extensive utilization of End Station A in competition with high energy experiments.

Our current judgment of relative priorities among the various demands on capital monies available to the elementary particle physics high energy physics program is such that we would not give your proposal sufficient priority to compete for such monies successfully. We therefore approve fully your plan to submit your proposal to the NSF and DOE medium energy nuclear physics programs for funding. If such funding were available then SLAC would be willing and able to conduct the

installation on a cooperative basis, to be agreed, subject to appropriate financial arrangements. Let me emphasize again, as noted in the letter of Mr. Rickansrud to you dated March 21, 1978, attached to your proposal, that the costs as furnished by SLAC are estimates only and actual costs may well differ. Moreover, the applicable administrative loading to the costs must be agreed to following discussions, by yourself, SLAC and the DOE (and NSF, if they were the funding source) staff involved.

A further matter concerns schedule. If your proposal schedule is approved and funded, the installation can commence during the anticipated summer shut down during calendar year 1979. However, we do not anticipate that it will be possible to complete the installation during that period, and continued installation is not compatible with operation of SLAC. We do not have a firm time table on scheduled shut downs beyond 1979. However, if we anticipate a summer shut down in 1980, then the installation work of the proposed off-axis injector could be completed during that summer. Testing could be done in the subsequent winter and therefore scheduled running cannot be anticipated before mid-1981.

Considering the above time table, it seems to me too premature to submit your proposal now to the PAC since that committee would have to consider your proposal in competition with other demands on the high energy physics facilities at SLAC as they will exist at the time of running. Moreover, we tend to instruct the PAC (although there can be justified exceptions) not to commit our facilities substantially beyond two years. In addition, it is planned to reorganize the PAC into the EPAC beginning next year, which will have advisory responsibility for the entire SLAC program, that is, the linear program, SPEAR and PEP. However, once funding is obtained and if a time table for installation has been agreed on, then it would be entirely appropriate for you to submit your proposal for consideration by the EPAC. As you suggest in your letter, you believe that electron scattering experiments on the lightest nuclei out to the largest momentum transfer available should stand up well in competition based on considerations of high energy elementary particle physics. The decision reached at the time such a proposal would be considered by the EPAC would, of course, depend on the total demands on SLAC resources, total available running time and particularly as it relates to End Station A. One could consider, once this new facility is installed, to change the arrangement under which proposals for running at the lower energy beam would be considered. However, according to your letter and also according to our views, it is neither your desire nor our wish to change the basis of program decisions for the low energy beam for the first running in such a beam and in particular not for the experiments discussed in your proposal.

As I noted above, it is desirable that this entire matter be discussed with the SPC before you could consider these replies to the questions in your letter as final. SPC will meet early this fall (either October 6 & 7 or September 23 & 24). However you are free to go forward with submitting your proposal to the Federal Agencies within the terms of this letter. I wish you all success.

With best personal regards,

W. K. H. Panofsky
Director

cc: W. Wallenmeyer
G. Charlton
B. Chertok
SPC members
E. Rickansrud
J. Ballam
R. Neal
S. Drell

THE AMERICAN UNIVERSITY
WASHINGTON, DISTRICT OF COLUMBIA 20016

College of Arts and Sciences
DEPARTMENT OF PHYSICS

October 11, 1978

Dr. W. K. H. Panofsky
Director, SLAC
2575 Sand Hill Road
Menlo Park, California 94025

Dear Pief:

I just had a short conversation with Bill Kirk who relayed to me the general conclusions by the SPC from their meeting of October 6 and 7, 1978, regarding the American University proposal for a new injector at SLAC. My understanding is that:

A) If we can get the money, SLAC will build Injector East.

B) If we need approval for a specific experiment before we can obtain funding, then we can proceed to the EPAC to request approval.

It would be helpful to me to have a short statement of the SPC recommendations from you in writing that I can use in my discussions with the funding agencies.

We are pleased with the SPC recommendations as we understand them, and we would like to proceed now to the next step. Since this project requires at least two years lead time before physics could begin, and since it is imperative to make requests for funding as early as possible, we would like to proceed at the earliest possible date to the EPAC with our proposal. If you think it desirable, I would like to arrange a meeting at your convenience to discuss with you what to present to the EPAC and at what time.

Sincerely,

Raymond G. Arnold

Raymond G. Arnold

RGA:wh

STANFORD UNIVERSITY

STANFORD LINEAR ACCELERATOR CENTER

Mail Address
SLAC, P. O. Box 4349
Stanford, California 94305

October 16, 1978

Dr. Raymond G. Arnold
Department of Physics
The American University
Washington, D. C. 20016

Dear Ray:

Thanks very much for your letter of October 11. Your presentation to the SPC was very valuable and I believe that the SPC will recommend that SLAC proceed along the lines which are now our current thinking. However, I can, of course, not guarantee the outcome of the SPC deliberations but they will report shortly.

SLAC's own position, pending SPC advice, is very similar to that outlined in your letter of October 11. Specifically:

1. If construction money for the Injector East can be obtained SLAC will indeed build it, although the schedule may not be as fast as some might wish. The schedule problems have been outlined to you in our earlier letter.

2. Any specific experiments, either using or not using Injector East, which your group wishes to propose to SLAC will go before the EPAC to advise the Director concerning approval.

3. The matter of nuclear structure physics experiments which might not be approved under the above procedure is a matter for further policy discussion which remains unanswered and is currently not in need of answer.

It would be a good idea for us to get together, but I suggest we do this after I have received the formal SPC recommendations. As you know the SPC is not advisory to the Director of SLAC but to the President of Stanford University, and we are maintaining those formal channels. However, of course, as soon as the SPC report has been received I will advise you of the relevant recommendations.

With best regards,

W. K. H. Panofsky
Director

cc: J. Ballam
S. Drell
W. Kirk

ABSTRACT

We propose to do elastic electron scattering from deuterium at forward and backward angles in the Q^2 range 0.6 to 2 $(GeV/c)^2$ and inelastic scattering from 0.4 to approximately 5 $(GeV/c)^2$ at the Stanford Linear Accelerator Center End Station A. From these data we will extract the magnetic structure functions $B(Q^2)$ and $2MW_1(Q^2, \nu)$. We will use the 1.6 GeV spectrometer at angles 37 to 155 degrees to measure electrons scattered from long liquid targets. For elastic scattering, the 8 GeV spectrometer will be used in coincidence to detect the recoil deuterons. To provide high intensity electron beams (50 to 100 mA peak) in the required energy range 0.4 to 2.9 GeV/c we propose that a new off-axis gun and in-line injector be built and installed in the SLAC linac at Sector 26.

We request a total of 970 hours of electron beam at 180 pps (including 75% efficiency) using the last 5 sectors of the linac to make elastic and inelastic scattering measurements.

CONTENTS

Section		Page
	Abstract	ii
	List of Figures	vi
	List of Tables	ix
I.	INTRODUCTION	1
	A. The Experiment	1
	B. The Motivation	3
	C. The Basic Requirements	4
	D. The Experimental Strategy	6
	E. The Future	7
II.	PHYSICS MOTIVATION AND POSSIBLE RESULTS	9
	A. Elastic Scattering From the Point of View of Nuclear Physics, $0.6 < Q^2 < 2$ (GeV/c)^2	9
	i) Previous Experiments	10
	ii) The Nonrelativistic Impulse Approximation	11
	iii) The Relativistic Impulse Approximation	12
	iv) Beyond the Impulse Approximation	16
	v) Meson Exchange Currents	17
	vi) Isobar Currents	20
	vii) Possible Experimental Results	21
	viii) Summary of Motivations for Measuring $B(Q^2)$	23
	B. Threshold Inelastic Scattering from the Point of View of Nuclear Physics, $0.4 < Q^2 < 2$ (GeV/c)^2	23
	i) Basic Ideas in Backward Threshold Deuteron Electrodisintegration	23
	ii) Previous Measurements at Low Q^2	25
	iii) Early Theory - Impulse Approximation and Meson Exchange Currents	25
	iv) Theoretical Questions at Larger Q^2	27

II. PHYSICS MOTIVATION AND POSSIBLE RESULTS (Cont.) Page

v) Some Predictions at Larger Q^2 28
vi) Possible Experimental Results 32
vii) Summary of Motivations For Measuring Backward Threshold Inelastic Scattering in the Range $0.4 < Q^2 < 2$ $(GeV/c)^2$ 33

C. Quasi Elastic Scattering $0.4 < Q^2 < 2$ $(GeV/c)^2$. 34

D. Elastic and Inelastic Scattering at Large Q^2, $Q^2 > 1$ $(GeV/c)^2$ - Quarks in the Deuteron. 36

i) The Experiment at Large Q^2 36
ii) Basic Ideas About Quarks in the Deuteron
a. Elastic Scattering 37
b. Inelastic Scattering 44
iii) Elastic-Inelastic Connection 46
iv) Six-Quark Coupling Calculations and the Possibility of Hidden Color in the Deuteron 46
v) Some Predictions at Large Q^2 50
vi) Possible Experimental Results 51
vii) Summary of Motivations for Backward Angle Scattering at Large Q^2 53

III. THE EXPERIMENT 55

A. Experiment Design 55

i) Overall Plan 55
ii) Beam 58
iii) Target and Scattering Chamber 59
iv) Spectrometers 60
v) Beam Dump 63
vi) Electronics and Computer 64
vii) Analysis 65
viii) Errors 66

B. Run Plans 68

Page

IV. POSSIBLE FUTURE PROJECTS 76

A. Experimental Facility Developments 76

B. Future Experiments 77

i) Physics Motivation 77

ii) The Experiments 81

iii) Possible Results 86

APPENDIX A - INJECTOR EAST 89

APPENDIX B - MONOCHROMAT 95

REFERENCES 98

ATTACHMENTS

FIGURES

		Page
II.1	Contributions to the deuteron $A(Q^2)$ in the Reid soft-core model	9
II.2	Existing data for $B(Q^2)$ together with various predictions	10
II.3	Nonrelativistic deuteron wave functions u(r) and w(r)	12
II.4	Nonrelativistic impulse approximation predictions for $B(Q^2)$	13
II.5	Relativistic impulse approximation predictions for $B(Q^2)$	15
II.6	Diagrams for e-d elastic scattering	17
II.7	Deuteron $A(Q^2)$ and $B(Q^2)$ using Reid soft-core with isobar current contributions	20
II.8	Previous and possible data for the deuteron $B(Q^2)$	21
II.9	Schematic of a typical spectrum of electrons scattered at backward angles from deuterium	25
II.10	The cross-sections for 180° deuteron electrodisintegration near threshold.	26
II.11	Diagrams for deuteron electrodisintegration	27
II.12	Reid hard-core matrix elements for processes contributing to deuteron electrodisintegration at 180° for E_{np} = 3 MeV	29
II.13	Reid hard-core double differential cross section for electrodisintegration at 180° for E_i = 400 MeV.	29

Page

II.14 Deuteron electrodisintegration cross section near threshold for back-scattered electrons at low Q^2. 30

II.15 Deuteron electrodisintegration cross section near threshold for back-scattered electrons at high Q^2 31

II.16 Deuteron electrodisintegration cross section at 180° from Sommer. 32

II.17 Schematic picture of electron-deuteron cross sections from the elastic to the deep inelastic regions 38

II.18 Elastic electromagnetic form factors of hadrons divided by the dimensional scaling quark model. 40

II.19 The deuteron form factor $F_d = \sqrt{A}$ divided by the quark interchange prediction. 40

II.20 Quark diagrams for elastic form factors for three-quark and six-quark hadrons 43

II.21 The deuteron inelastic structure function $F_{2D} = \nu W_2$ 45

II.22 The deuteron form factor $A(Q^2)$ assuming 2% probability for the six-quark state 47

II.23 The deuteron form factor $B(Q^2)$ assuming 2% probability for the six-quark state 48

II.24 Curves of equal baryon density for the six-quark MIT bag model 49

II.25 Two nucleon interaction energy vs. the constrained baryonic quadrupole moment Q for the six-quark system in the MIT bag model 49

II.26 Overview of the range of predictions for the deuteron structure function $2MW_1$. 52

Page

III.1 Plan view of the proposed experimental layout. 56

III.2 Kinematic regions for elastic scattering and low and high Q^2 threshold inelastic scattering 57

III.3 Kinematic region for quasielastic scattering 58

IV.1 The magnetic form factor of ^3He. 79

IV.2 The magnetic form factor of ^3H 79

IV.3 The ^3He elastic structure function $A(Q^2)$ at large Q^2. 80

IV.4 Previous and possible data for ^3He F_{mag} 86

IV.5 Previous and possible data for ^3He F_{ch} 86

IV.6 Previous and possible data for ^3H F_{mag} 87

A.1 Schematic of the proposed Injector East. 92

A.2 Experimental measurements of Beam Breakup Threshold for a five-sector beam in the SLAC linac 93

B.1 Schematic of an energy compression system for the SLAC A-line. 95

TABLES

		Page
I.	Resolution for e-d single arm	62
II.	Estimated SLAC triplex computer resource requirements.	65
III.	Run plan for e-d elastic scattering	70
IV.	Run plan for low Q^2 threshold inelastic scattering	72
V.	Run plan for quasi elastic scattering	73
VI.	Run plan for high Q^2 threshold inelastic scattering	74
VII.	Requested number of hours of five-sector beam using Injector East at 180 pps.	75
VIII.	Typical values for energy loss d E/dx by incident electrons in ^{3}He and ^{3}H targets	83
IX.	Range of kinematic settings for e-^{3}He and e-^{3}H elastic scattering and typical values for beam energy spread	84

I. INTRODUCTION

A. The Experiment

The cross section for elastic electron scattering from a nuclear target can be written:

$$\frac{d\sigma}{d\Omega} = \sigma_M \left[A(Q^2) + B(Q^2) \tan^2(\theta/2)\right] \qquad \text{I.1}$$

The inelastic cross section may be expressed:

$$\frac{d\sigma}{d\Omega dE} = \sigma_M [W_2 + 2 W_1 \tan^2 (\theta/2)] \qquad \text{I.2}$$

In a recent series of experiments (A1-A5) the American University group has measured forward angle elastic and threshold inelastic electron scattering cross sections on d, ^{3}He, and ^{4}He and extracted the structure functions $A(Q^2)$ and νW_2. The range of momentum transfer from 0.6 up to, in some cases, 6 $(GeV/c)^2$ covered in these experiments spans the transition region from nuclear to quark physics. At the lower Q^2 the scattering is best described in terms of traditional nuclear physics with nucleons bound together by the exchange of virtual mesons; at the high Q^2 the internal structure of the nucleons begins to appear. The deuteron experiment (A1, A2) has stimulated considerable theoretical development towards an understanding of the short distance structure of the simplest nucleus. The results for ^{3}He and ^{4}He are just being published (A4, A5), and they promise to be an exciting stimulus for theoretical investigation of the three- and four-body nuclear systems at short distances. We are presently doing quasi elastic electron-deuteron scattering at large Q^2 to measure the neutron structure function (A6).

Equally important are the magnetic structure functions $B(Q^2)$ and $2MW_1$.

We are now proposing the following backward angle measurements using a deuterium target:

1. Double arm elastic scattering in the range $0.6 < Q^2 < 2\ (GeV/c)^2$ using the 1.6 GeV spectrometer to detect the scattered electrons in coincidence with the recoil deuterons in the 8 GeV spectrometer. Measurements at two angles will be taken at each Q^2 and the magnetic structure function will be extracted in a Rosenbluth separation.
2. Single arm threshold inelastic scattering using the 1.6 GeV spectrometer to measure the cross section at 155° and a forward angle at several Q^2 values in the range $0.4 < Q^2 < 2\ (GeV/c)^2$. Rosenbluth separations of the electric and magnetic structure functions will be made.
3. At three settings of the incident energy the inelastic measurement will be extended from threshold over the entire quasi-elastic peak.
4. Single arm threshold inelastic scattering at several Q^2 points in the region $Q^2 > 2\ (GeV/c)^2$ using the 1.6 GeV spectrometer at one far backward angle (155°).

This will give $R = \sigma_L/\sigma_T$ the ratio of longitudinal to transverse cross section, at and near the elastic peak for $Q^2 \leq 2\ (GeV/c)^2$. In the following section we give a brief overview of the physics to be explored. In Section II a more detailed description of the theories and models is given. At the end of each subsection there is a description of the possible results of this experiment and a short summary of the physics ideas to which the reader may refer for the essence of the arguments.

B. The Motivation

A satisfactory understanding of nuclear structure at short distances will require a consistent theory using relativistic nuclear wave functions with the possibilities for nucleon resonance admixtures and meson exchange (MEC) processes, all calculated with a proper treatment of couplings and vertex form factors. At the present time there does not exist such a complete calculation. However, it is clear that the acid test of such a theory, or even of various pieces in approximate calculations, will be to get good agreement with the electromagnetic structure functions of the simplest nuclear systems in the region $0.4 < Q^2 < 2$ $(GeV/c)^2$.

Backward angle scattering promises to be an even richer field in which to investigate the nucleon-nucleon (NN) interaction at short distances than were the forward angle experiments. Some of the important details of the basic NN interaction are more clearly revealed in magnetic structure functions at high Q^2 than in the electric ones. In particular, as will be explained in more detail in Section II, the meson exchange currents (MEC), which have often been singled out as an interesting piece of the nuclear-physics puzzle, may appear as big effects. This occures in the Q^2 range between 0.4 to 1.5 $(GeV/c)^2$ (10 to 40 $1/fm^2$) where the impulse approximation terms are predicted to be going through diffraction minima. Measurements of the magnetic structure functions of the light nuclei in that Q^2 range with an uncertainty of 5 to 10% will test for the existence of MEC contributions, and, if they exist, could yield important information on the details of those processes. This would be of major importance to our understanding of all nuclei at short distances.

At Q^2 above 1 to 2 $(GeV/c)^2$ the quark degrees of freedom may start to

become important. Here the momentum dependence of the elastic and threshold inelastic structure functions of nucleons and nuclei is a consequence of the approximately equal sharing of the momentum transfer among the quark constituents. The agreement of the predictions of the dimensional scaling quark model with the asymptotic shape of the structure function data for the hadrons π, p, and the d suggests that at Q^2 above about 1 to 2 $(GeV/c)^2$, the deuteron may be viewed as a coherent system of six-quarks (J1, J3). The data for the ^3He structure functions at Q^2 of 2.5 and 3.0 $(GeV/c)^2$ are consistent with a quark model prediction (A4, J11). A study of the magnetic structure functions $B(Q^2)$ and $2MW_1$ and a comparison of them with the forward angle structure functions $A(Q^2)$ and νW_2 promises to reveal information on the details of the way the quarks share the momentum transfer at high q. In particular, as will be described in Section II, to understand $2MW_1$ at and near the exclusive limit (elastic peak), explicit account must be taken of the spins of the quarks and gluons and the dynamics of the quark-gluon interaction.

C. The Basic Requirements

The major factors governing the design of the experiment are:

1. Scattering at backward angles (37 to 155°) from the A = 2 and 3 nuclei in the Q^2 range 0.4 to 6 $(GeV/c)^2$ requires the electron beam energy range to be approximately 0.4 to 2.9 GeV/c.
2. The backward elastic cross sections are expected to be around 10^{-36} to 10^{-40} cm^2/sr in the Q^2 range 0.4 to 2 $(GeV/c)^2$, and similarly for the threshold inelastic cross sections.

These facts indicate that to perform successful backward angle scattering experiments at high Q^2 in a reasonable amount of running time it is absolutely necessary to have a high intensity electron beam in the energy range 0.4 to 2.9 GeV/c and to use thick targets and big solid angles to maximize the counting rate. At the present time there is no electron accelerator anywhere that can produce high intensity electron beams in the required energy range. SLAC has the energy, but at present the yield of beam current is limited by beam breakup phenomena to around 5 to 10 mA peak in the region of 2 GeV, falling to about 1 mA with poor beam quality around 1 GeV, and nothing below about 800 or 900 MeV. During E101 we made one measurement (A3) of $B(Q^2)$ at Q^2 = 1.0 (GeV/c)2 using this low quality beam at about 900 MeV. The results were marginal (See Fig II.1), but that experience showed us a hint of what could be done given a better beam.

Therefore, we are proposing that an off-axis gun and in-line injector be constructed and installed in Sector 26 of the linac which will produce an electron beam in the range 0.4 to 2.9 GeV with maximum beam currents limited by beam breakup in the range 50 to 100 mA peak (13.5 to 27 μA average current at 180 pps). (See Appendix A and Fig. A.1.) This is an increase of as much as a factor of 100 over what is presently available in the required energy range at SLAC. With such high beam intensities, together with the splendidly equipped ESA spectrometers, counting house and facilities for long liquid and gaseous targets, we can make backward angle elastic (inelastic) electron scattering measurements in light nuclei down to the level of 10^{-40} cm^2/sr (10^{-40} $cm^2/sr/MeV$). This will allow us to probe the deep magnetic structure of nuclear matter through the transition region from the domain where nuclear physics descriptions prevail to the level where the

quark degrees of freedom may become important.

D. The Experimental Strategy

Assuming we have sufficient beam intensity in the useful energy range, what is the best strategy for measuring the magnetic structure functions?

The ideal way to measure the term $B(Q^2)$ or $2MW_1$ in the Rosenbluth equations I.1 and I.2 is to detect the scattered electrons at 180°. In practice it turns out that scattering at several angles away from 180° has several advantages over 180° scattering in the situation where the cross sections are small.

1. For elastic scattering, the recoil nuclei can also be detected and a double arm coincidence can be used. This is an enormous advantage because a coincidence measurement can pick out a small elastic signal clearly without making all the sacrifices necessary to preserve good enough resolution (better than 1 MeV) to do it in single arm. For a coincidence experiment the beam and spectrometer resolution requirements are less stringent, and long targets can be used without worrying about loss of resolution from energy straggling.
2. Since the target is viewed from the side, it can be long (40 cm) even for single arm experiments. A correction can be made for the energy straggling of the incident electrons using the reconstructed position of the scattering along the target length. The resulting resolution in E_f (2 to 3 MeV) is good enough for inelastic scattering measurements. For scattering at 180° the electrons must traverse (on average)

the entire length of the traget, and there is no way to make a correction for energy straggling. This limits the target length to about 1 cm for a resolution of 1 MeV, which puts an intolerable limit on the counting rates.

3. The physical arrangement of the beam transport and spectrometer is much simpler. Scattering at 180° requires special beam transport systems not readily adaptable to the circumstances in ESA, whereas the present setup is nearly ideal for 37 to 155° measurements and for coincidence experiments.

A major consideration in the design of a Rosenbluth separation experiment is to keep the differences in systematic errors small between the forward and backward angle measurements so that shallow slopes on the Rosenbluth plots can be measured with good confidence. This requirement is well satisfied by making the forward and backward measurements in the same instrument, such as the 1.6 GeV spectrometer, with a minimum of changes of experimental conditions. Since the counting rates at the forward angles are relatively high, those points make a small impact on the overall experiment design and on the running time budget. The major emphasis in the experiment design and the run plan, described in Section III, is to maximize the yield from the backward angle measurements.

E. The Future

The present proposal is to do elastic and inelastic backward angle measurements on the deuteron. This target is chosen because it is the simplest nucleus, the one for which the most detailed theoretical investiga-

tions have been done, and the one where the interesting effects due to exchange currents, relativistic wave functions, possible isobar configurations, nucleon form factors and the quark constituents are most likely to be evident with the least complications.

We are also interested in future experiments to separate the charge and magnetic structure functions, F_{ch} and F_{mag}, of the A = 3 nuclei, ^3He and ^3H, at high Q^2. They promise to be a rich source of information about meson exchange currents, relativistic three-body wave functions, neutron structure functions, possible three-body forces, and other aspects of the NN interaction at short distances. The comparison with theory can best be made when F_{ch} and F_{mag} are separately known. As is the case in the deuteron, the interesting and more exotic effects manifest themselves most often as a shift or a filling in of the diffraction features predicted by the impulse approximation, in some cases with opposite effects in ^3He and ^3H.

Once the new injector is built, these experiments could be done using a straightforward extension of the techniques proposed here in Section III for the deuteron, with only minor additional capital expenditures. The physics questions and possible results from such experiments are described in Section IV.

II. PHYSICS MOTIVATION FOR LARGE Q^2 BACKWARD ANGLE e-d SCATTERING.

A. Elastic Scattering From the Point of View of Nuclear Physics

The deuteron $A(Q^2)$ structure function is composed of contributions from all three form factors, G_C, G_Q, G_M (See Fig. II.1). It just happens that about 25 $1/fm^2$ where the charge form factor G_C is predicted to be going through a diffraction minimum, the predicted quadrupole form factor G_Q is large and completely fills in the minimum. Variations in the size and shape of the basic ingredients such as relativistic wave functions, meson exchange currents, isobars, and the neutron electric form factor G_{En} cause shifts in the size and position of the diffraction features of the individual form factors that are generally obscured in the total $A(Q^2)$. Various models with different diffractive shapes for G_C and G_Q yield similar smooth shapes for $A(Q^2)$. Consequently, until G_C and G_Q are separately determined in a deuteron polarization experiment, we are faced with trying to distinguish between various models from the overall shift up or down in $A(Q^2)$. This situation is

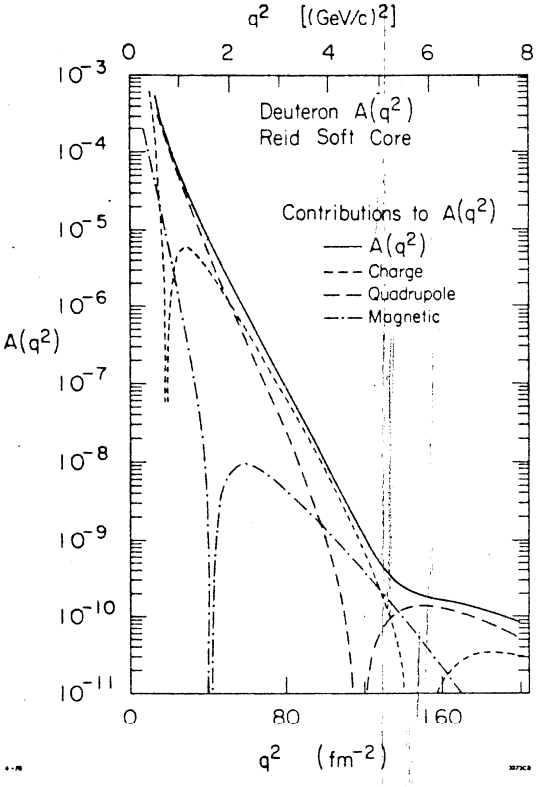

Fig. II.1. Contributions to the deuteron $A(Q^2)$ in the Reid soft-core model.

appropriately called the Gordian Knot by Gari and Hyuga (D2). Measurements of the $B(Q^2)$ structure function, as we will show in the following, may help in untangling the Knot.

i) Previous Experiments

$0.5 < Q^2 < 2.\ (GeV/c)^2$

The present data at low Q^2 on the deuteron $B(Q^2)$ comes mostly from measurements made in the 1960's (B1-B5). The data of Buchanan and Yearian (B4) and of Rand et al., (B5) from Stanford extends only up to $Q^2 = 14\ 1/fm^2$. The highest Q^2 data is one point at $Q^2 = 1.0\ (GeV/c)^2$, with rather large error bars, that we have measured at SLAC (A3). (See Fig II.2). Unfortunately, the relatively low Q^2 and the size of the experimental errors on the existing data do not allow a clean distinction to be made between the competing calculations. As we will see below, more interesting possibilities open up at larger Q^2.

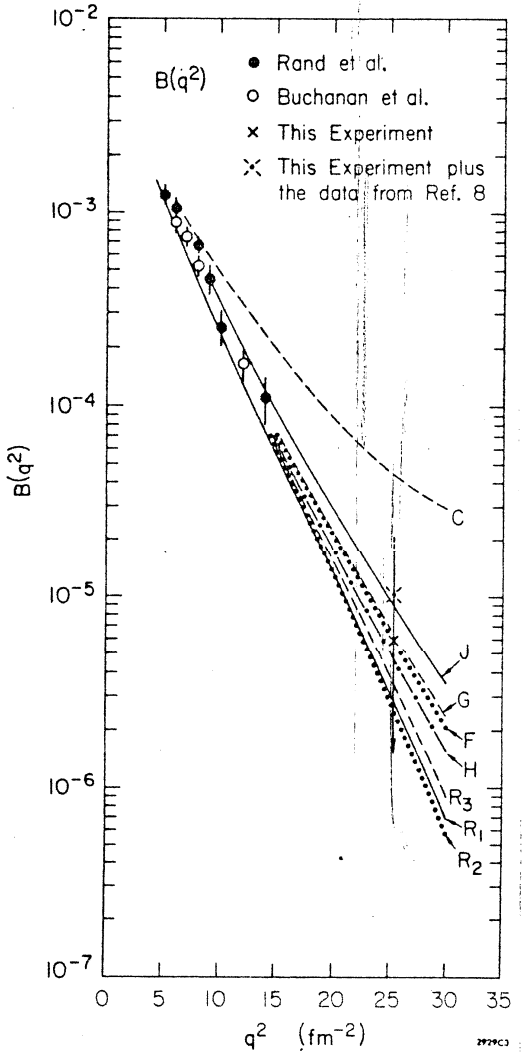

Fig. II.2. Existing data for $B(Q^2)$ together with various impulse and MEC predictions from Ref. (A3) where the curves are explained in more detail.

ii) The Nonrelativistic Impulse Approximation

The electron scattering at moderate Q^2 can be viewed as a probe of the moments of the charge and current distributions inside the nucleus. Backward scattering is a probe of the spacial distribution of the electric current and magnetization densities (K2). In the nonrelativistic impulse approximation (NRIA), i.e., one photon exchange connecting to only one nucleon, there is a contribution to the magnetic scattering from the convection current due to the moving nucleons and from their intrinsic magnetic moment distributions. A nonrelativistic description of the spin-1 deuteron using the Schroedinger equation contains two wave functions, u and w, giving the probability for the two nucleons to be moving in a relative S or D state. The elastic magnetic structure function in the NRIA is given by the following:

$$B(Q^2) = \frac{4}{3}\eta(1+\eta)\, G_M^2(Q^2) \qquad \text{II.1}$$

where

$$G_M = \frac{M_d}{M_n}\left[G_{MS}\, C_S + \frac{1}{2}\, G_{ES}\, C_L\right]$$

$$C_S = \int_0^\infty \left\{ \left[u^2(r) - \frac{1}{2}\, w^2(r)\right] j_0(Qr/2) + \frac{w(r)}{\sqrt{2}}\left[u(r) + \frac{w(r)}{\sqrt{2}}\right] j_2(Qr/2) \right\} dr$$

$$C_L = \frac{3}{2}\int_0^\infty w^2(r)\left[j_0(Qr/2) + J_2(Qr/2)\right]\, dr$$

Presently, there are a large number of models of the NN potential (F1-F5) derived from NN phase shifts and the two-body data. The deuteron

wave functions can be obtained from these models (See Fig. II.3) and used to calculate the NRIA contribution to magnetic scattering By Eq. II.1.

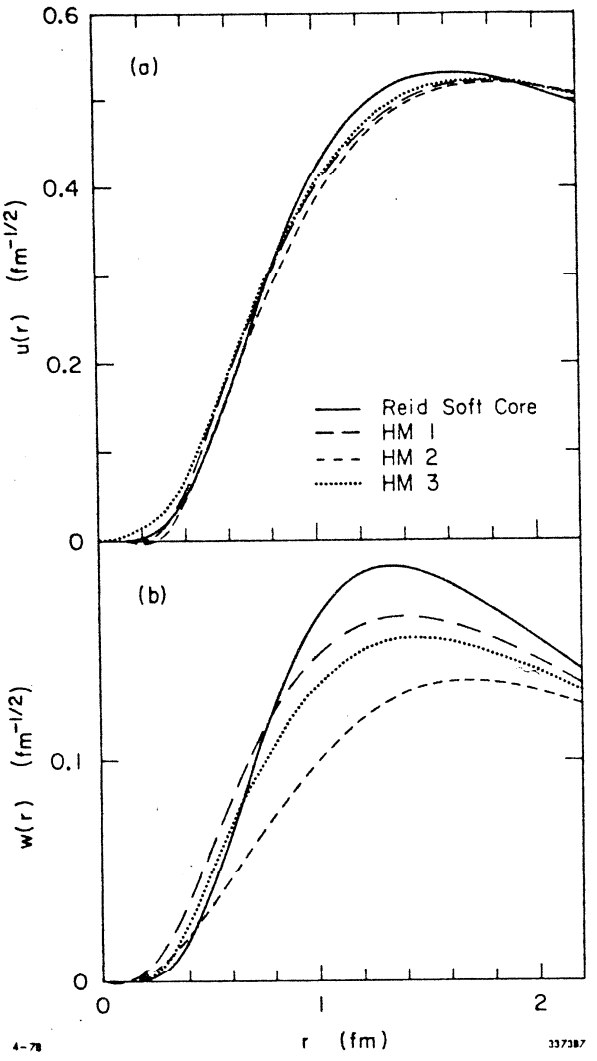

In Fig. II.4 are plotted curves for $B(Q^2)$ from several nonrelativistic deuteron models. In each case we observe a diffraction feature with a minimum in the region of Q^2, 30 to 50 $1/fm^2$. The shape of the diffraction feature is primarily determined by the D state wave function w(r). The S state functions, u(r), for these models are nearly all alike, while the D states differ considerably in the region 0.5 to 2.5 fm, as shown in Fig. II.3.

Fig. II.3. Nonrelativistic deuteron wave functions from the N-N potential models of Reid (F2) and Holinde-Machleidt (F3,F4): a) the S state, b) the D state.

iii) The Relativistic Impulse Approximation

The NRIA is expected to break down when Q^2 becomes large, say as big as the mass of the nucleon. A fully covariant description of the scattering process would naturally include the effects due to the relativistic kinematics, such as Lorentz contraction of the rest frame deuteron wave

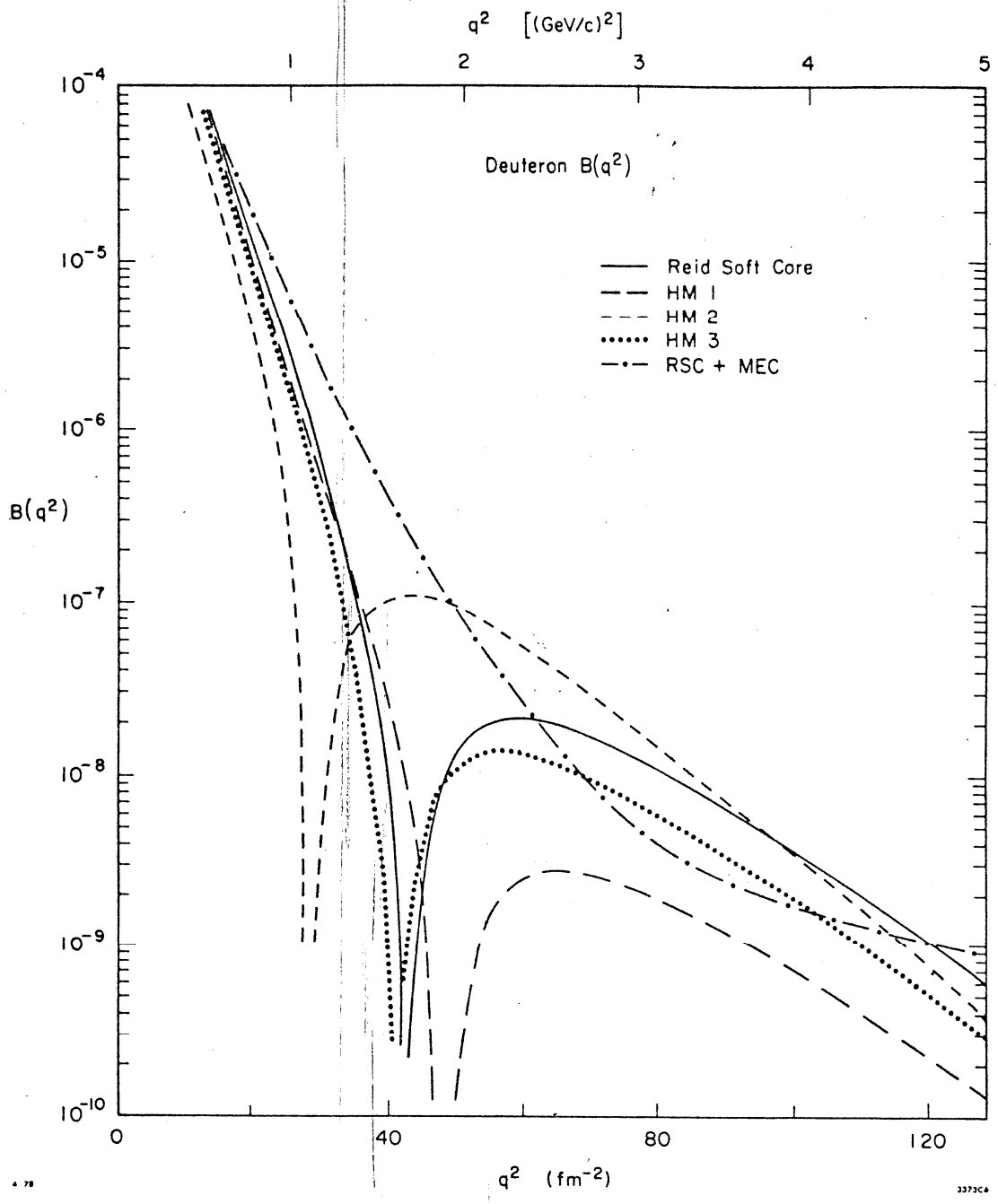

Fig. II.4. Nonrelativistic impulse approximation predictions for $B(Q^2)$ using dipole nucleon form factors. The curves are: Reid soft-core (F2); HM1, HM2, HM3, the N-N potential models of Holinde and Machleidt (F3, F4); RSC and MEC, the calculation of Gari and Hyuga (D3) using Reid soft-core plus meson exchange.

functions due to recoil and precession of the spins, and would also provide for the creation and annihilation of particles. There are several recent relativistic impulse approximation (RIA) calculations of the deuteron structure functions, each starting from a different point of view (E1-E5). We sketch here two of those calculations to indicate the theoretical progress being made in this area. The main point for our proposal is that the real test of these relativistic calculations can only be made at large momentum transfer, as in the region where we are proposing to measure $B(Q^2)$.

Gross's Theory - In Ref. D1 the elastic deuteron structure functions were calculated using a formalism developed by F. Gross in which the spectator nucleon is kept on the mass shell while the struck nucleon is allowed to go off the mass shell. This is a fully relativistic calculation, i.e., not an expansion in Q^2/m^2, done in the framework of nuclear physics. It uses deuteron models with four-component wave functions instead of only two components. The additional P state wave functions are associated with the negative energy states of the off-mass-shell nucleon. They are determined by Gross (E6) along with modified u and w wave functions in a self consistent solution of a relativistic equation for the n-p-d vertex, which depends on certain parameters describing the meson-N-N couplings. The P-state negative energy wave functions include part of what has been calculated by other people as a meson exchange current, as we will discuss further below. The main point is that this theory could provide a rather complete description of the high momentum transfer scattering from the point of view of nuclear physics without the obvious approximations of the non-relativistic calculations. Therefore, the comparison of this theory with

the data may be a good test of the input to the theory (wave functions, percent D state, G_{En}, etc.).

Gross's results for $B(Q^2)$ for several choices of the coupling parameter are compared with the Reid soft-core NRIA model in Fig. II.5. In each case we observe $B(Q^2)$ with a sharp diffraction feature at about 25 to 45 1/fm2. The position of the minimum and the height of the second maximum are different in each, but the basic diffraction feature is always present.

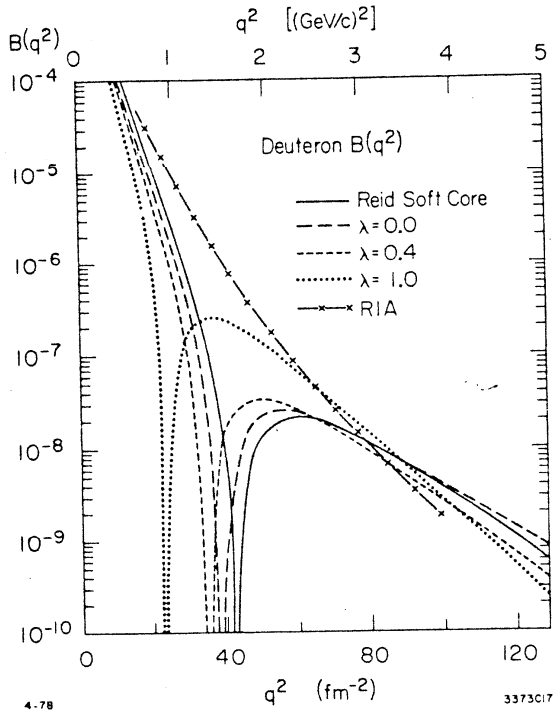

Fig. II.5. Relativistic impulse approximation predictions for $B(Q^2)$ compared with the Reid model. The curves by F. Gross (E1, E6) are labeled by the mixing parameter λ. For $\lambda = 0$ the $\pi - N$ coupling is pure $\gamma_5\gamma_\mu$, for $\lambda = 1$ it is pure γ_5. The The curve labeled RIA is by Fernandez-Pacheco, et al.,(E3).

Schmidt et al., Theory - The recent paper by Fernandez-Pacheco, Grifols, and Schmidt (E3) is an extension of the RIA models by Schmidt and Blankenbecler (J4, J5) to include the deuteron spin. They are primarily interested in the very high momentum transfer region, and they use infinite momentum frame techniques to construct a model that gives deuteron form factors with the same asymptotic shape as that given by the quark counting rules. The two parameters of their model are determined by fits to the deuteron elastic structure function data at lower Q^2. Their prediction for

$B(Q^2)$ is shown in Fig. II.5 where we see a smooth curve with no diffraction features, in complete contradiction to the nonrelativistic models and to the relativistic calculation by Gross.

iv) Beyond the Impulse Approximation

If the impulse approximation were the complete picture, we could regard large Q^2 e-d scattering as a probe of the short distance behavior of the relativistic deuteron wave functions, and we would consider the experiments as testing the assumptions of models like the ones just described. Alternatively, we might try, as has been done in the past at lower Q^2, to use the best available deuteron models as a basis for extracting the neutron elastic form factors from the e-d data, assuming the other uncertainties were small.

However, we know that even the relativistic impulse approximation is not the complete picture and that other currents besides the ones due only to the nucleons are expected to show up. At least two other types of currents can be identified in the nuclear-physics language. One is the currents carried by the exchange of virtual mesons that are responsible for the NN potential, the so called meson exchange currents (MEC). Another is due to the possibility that the internal degrees of freedom of the nucleons themselves can be excited by high momentum collisions with other nucleons in the nucleus. Thus, the virtual photon might "see" a momentarily virtual nucleon isobar, whence the name isobar currents (IC). Possible diagrams for the contributions of the impulse, exchange, and isobar currents to e-d elastic scattering are shown in Fig. II.6.

Finally, at sufficiently large Q^2 we expect the whole nuclear-

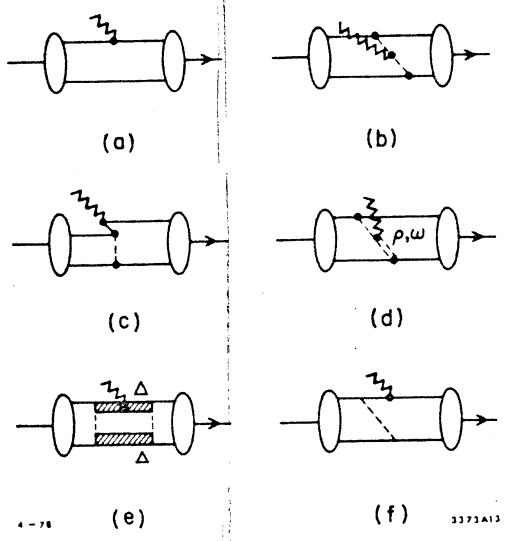

Fig. II.6. Diagrams for e-d elastic scattering: a) impulse approximation; b) single pion exchange (not allowed); c) pair term; d) $\rho\pi\gamma$ or $\omega\pi\gamma$ exchange; e) isobar term; f) recoil term.

physics approach to break down, and theories which explicitly take into account the quark structure of the nucleons should become more appropriate. To date, most of the quark models are not as detailed as the nuclear physics calculations. So far they only offer predictions for the shape of $B(Q^2)$ as a function of Q^2 or compared to $A(Q^2)$, and then only for asymptotic Q^2 (wherever that is!!). There is, however, one explicit calculation of $A(Q^2)$ and $B(Q^2)$ using a six-quark model of the deuteron by Kobushkin (J8). His results are shown in Fig. II.20 for $A(Q^2)$ out to Q^2 of 160 1/fm2 (6 $(GeV/c)^2$) and in Fig. II.21 for $B(Q^2)$ out to Q^2 of 30 1/fm2 (1.2 $(GeV/c)^2$). The reader should compare that prediction with the nuclear-physics calculations we are describing here. We postpone until Section II.D a more detailed discussion of the quark model predictions for $B(Q^2)$.

v. Meson Exchange Currents

The deuteron is isoscalar, I=0. If the virtual photon is to connect to any number of pions and then to the deuteron, those pions must have I=0. The G parity conservation limits the γ-meson interaction in the deuteron

to a system of an odd number of pions. This means that elastic e-d scattering will not be able to "see" the most important long range isovector one-pion exchange current, Fig. II.6b. Elastic e-d scattering will only connect to isoscalar systems like $\rho\pi$, $\omega\pi$, etc., as in Fig. II.6d, where the ρ and ω are considered as multipion resonances. If isoscalar MEC contribute significantly to elastic e-d scattering, this might be a clean place to study just them without complications from other possibly larger isovector processes. To date there is no CLEAR experimental evidence for or against the existence of isoscalar exchange currents in the deuteron.

The deuteron inelastic structure functions, on the other hand, can receive contributions from isovector exchange currents, because in the electrodisintegration there is no requirement for the final state to have isospin I=0. We will see in Section II.B that isovector MEC can make large contributions to the electrodisintegration in certain kinematic regions. Thus, elastic and inelastic e-d scattering may be complimentary ways to probe different details of the exchange currents.

There now exist several calculations of the deuteron elastic structure functions including MEC. We will show results here only from the work of Gari and Hyuga (GH)(D2), which is the most complete calculation out to large Q^2 (200 $(1/fm)^2$). The others give similar results at lower Q^2. In Fig. II.4 we show the GH result for $B(Q^2)$ (the curve labeled "RSC + MEC") compared with several nonrelativistic impulse calculations. Gari and Hyuga have included isoscalar currents corresponding to the diagrams of Fig. II.6c and II.6d, but not the disputed recoil term of Fig. II.6f. They have also included phenomenological form factors at the meson-N-N verticies which are important at large Q^2 where they damp the exchange process.

As Fig. II.4 shows, the effect of the isoscalar exchange current contributions is to completely fill in the diffraction minimum in $B(Q^2)$ around 40 $1/fm^2$. Thus, a measurement in the region 25 to 50 $1/fm^2$ (1 to 2 $(GeV/c)^2$) would be an excellent probe of the isoscalar MEC, and might be used to distinguish various details of these currents if they are as large as the GH prediction. On the other hand, it is possible that a measurement of $B(Q^2)$ would fall quickly with Q^2 following the impulse predictions and perhaps even show a sharp diffraction feature. Such a result would establish a severe limit on the allowed size of the isoscalar MEC contributions and would force a reassessment of the basis for the MEC predictions.

In the calculation of GH (D2), the largest contribution to the exchange terms for $A(Q^2)$ up to $Q^2 = 2$ $(GeV/c)^2$ comes from the so-called "pair" term with a pion exchanged, Fig. II.6c. There is some dispute over whether the pair term is properly described as a meson exchange current. F. Gross has argued (E4, E5, E7) that the pair diagram is really part of the relativistic deuteron wave function where the struck nucleon is allowed to have negative energy components. The exchanged meson is then just part of the normal NN potential and should not be considered as a separate MEC contribution.

In the magnetic structure function the $\rho\pi\gamma$ and the π-pair terms are about the same size at low Q^2, and the $\rho\pi\gamma$ term dominates above 25 $1/fm^2$ (1 $(GeV/c)^2$) (D3). Regardless of the view point about the pair term, the other undisputed isoscalar MEC terms, such as $\rho\pi\gamma$, are distinct from any confusion with the impulse terms. The main question to be answered by experiment is: Are they really present? If they are, then a measurement in the region of the diffraction minimum in $B(Q^2)$ might give important information on such details as : How many such exchange diagrams must be included?

What is the size of the γ-meson and meson-N-N coupling?: What is the Q^2 dependence of the meson-N-N form factors? If such a clean measurement in the deuteron were to establish the credibility of the isoscalar MEC processes, then these mechanisms might be used with better confidence to understand the structure of other nuclei.

vi) Isobar Currents

The subject of isobar currents in the deuteron and in nuclei in general is one that has received a good deal of attention in recent years (K3, K4). Such currents could arise from close collisions between bound nucleons leading to mutual virtual excitation of their internal degrees of freedom. This could give admixtures to the deuteron wave functions from excitation of virtual $\Delta(1236)$, $\Delta(1236)$ or $N'(1470)$, $N'(1470)$, etc., which might be present when the virtual photon comes probing.

There are two recent calculations (D3, D4) of IC contributions to e-d scattering for Q^2 up to 150 $1/fm^2$ (6 $(GeV/c)^2$). We show in Fig. II.7 the results from the work of Fabian and Arenhovel (D4). The results of Gari et al., (D3) are similar. The IC effects are largest, as indicated in Fig II.7, in the $B(Q^2)$ structure function in the region of the

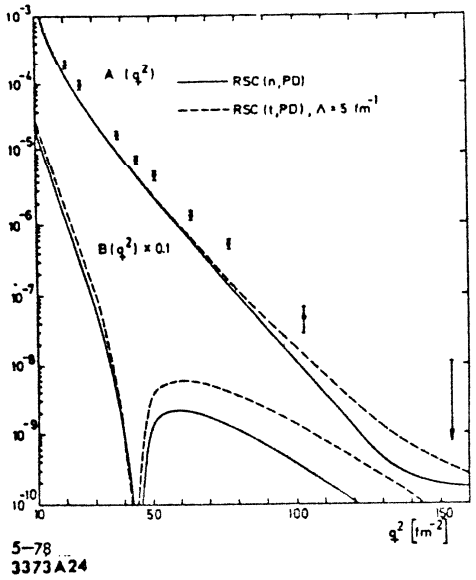

Fig., II.7. Deuteron structure functions $A(Q^2)$ and $B(Q^2)$ for Reid soft-core potential with and without isobar currents, from Fabian and Arenhovel (D4). Data points are from Ref. (A1).

second maximum above about 50 $1/fm^2$. The IC effects on $B(Q^2)$ are not as large as the predicted effect of isoscalar MEC, but the main point to notice is that the predicted IC admixtures do not destroy the basic diffraction feature. Therefore, if the MEC turn out to be small and a diffraction feature is observed, the measured $B(Q^2)$ may be sensitive to the presence of virtual isobars in the deuteron.

vii) Possible Experimental Results

Possible data for the elastic structure function $B(Q^2)$ using two hypotheses for the shape of the function are displayed in Fig. II.8. The error bars given there are the statistical errors only. Details of the proposed experiment are given in Section III. The counting times quoted in Table III, Section III, correspond to the points along the curve labeled "RSC and MEC" (Reid soft-core plus meson exchange currents). The limit of sensitivity to

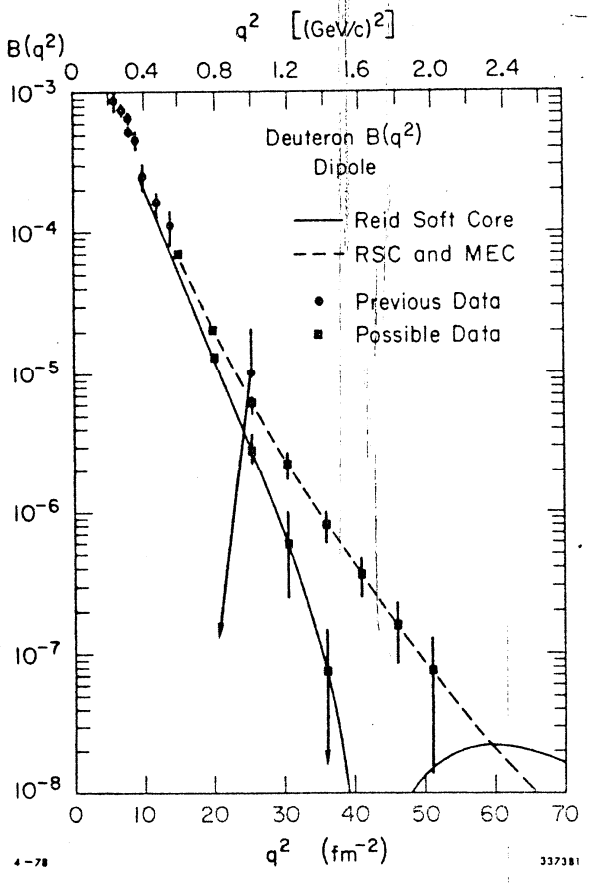

Fig. II.8. Possible data for $B(Q^2)$ according to two predictions for the cross section: Solid curve) Reid soft-core impulse approximation; dashed curve) Reid soft-core plus MEC by Gari and Hyuga (D2). Previous data are from Ref. (A3) and references therein.

$B(Q^2)$ is at about the 10^{-7} level, which will occur probably somewhere in the neighborhood of $Q^2 = 2$ (GeV/c)^2. Elastic scattering cross sections at backward angles can be measured at Q^2 larger than 2 (GeV/c)^2 in the proposed experiment out to limits of a few events per point, but the small Rosenbluth slopes cannot be determined from such data. For example, the possible data point in Fig. II.8 at $Q^2 = 2$ (GeV/c)^2 on the "RSC and MEC" curve corresponds to:

$$\left.\frac{B \tan^2(\theta/2)}{A}\right|_{\theta = 142°} = 0.12$$

Consequently, statistical errors smaller than 10% are required on the backward angle point to measure the Rosenbluth slope.

From Fig II.8 we see that the proposed experiment could determine if there were a diffraction feature with a minimum in the range $20 \leq Q^2 \leq 40$ 1/fm^2 and a second maximum at the level of 10^{-7} at higher Q^2, as predicted by several of the theoretical curves in Figs. II.4 and II.5. Such a diffraction feature could easily be distinguished from the situation with no diffraction minimum in that range as predicted by the meson exchange calculations. If the isobar currents behave as suggested in Fig. II.7, they could push the structure function in the region around 50 1/fm^2 even higher into our visibility without much contribution at lower Q^2.

Our measurement would extend the knowledge of $B(Q^2)$ down in sensitivity by about three orders of magnitude and perhaps double the range of Q^2 covered by previous experiments.

viii) Summary of Motivation for Measuring $B(Q^2)$

A primary purpose for the elastic scattering portion of our proposed experiment is to obtain evidence that would limit the range of possibilities for (relativistic?) deuteron wave functions, meson exchange, and isobar currents. Such evidence may be established relatively clearly from the diffractive features of the deuteron $B(Q^2)$. This would be of major importance, not only for the two nucleon system but also for other medium energy nuclear-structure calculations.

In Section II.D we discuss the motivation for measuring $B(Q^2)$ to as large a Q^2 as possible to test the quark ideas in the approach-to-scaling region.

B. Threshold Inelastic e-d* From the Point of View of Nuclear Physics, $0.4 < Q^2 < 2$ (GeV/c)^2

i) The Basic Ideas in Backward Threshold Electrodisintegration

Electro (and photo) disintegration of the deuteron (e-d*) has long been used to probe the details of the NN potential and the electromagnetic interaction with nuclear matter. Threshold deuteron e-d* at backward angles has for some time been known to be an especially rich area. Physically this can be understood in the following simplified picture. An electron scattering at backward angles emits primarily a magnetic photon (pure magnetic at $\theta = 180°$) with $J = 1$ and $P = +1$. Such a transverse photon induces primarily magnetic (spin flip) transitions in the target. Threshold disintegration of the deuteron (BE = 2.2226 MeV) leaves the neutron and proton unbound with low relative energy (E_{np} of a few MeV) and the centrifugal barrier suppresses all but the lowest angular momentum final states. The magnetic character of the

photon and the preference for S wave final states means that the dominant contribution right at threshold comes from the nucleon spin flip transition from the I = 0 $^3S_1$ and $^3D_1$ states to the ^1D_o state with I = 1. Near threshold the unbound mixture of $^3S_1$ and $^3D_1$ (called the α state) also contributes. Farther from the threshold increasingly higher angular momentum final states come in until, in the region of the quasi elastic peak, the outgoing nucleons leave in essentially plane waves. In this simple picture we can see several advantages of studying backward angle e-d* near threshold (up to three to four MeV above breakup):

1. The process is relatively simple, i.e., primarily magnetic with few partial waves. Therefore, the theoretical calculations should be easier than for the case where many partial waves contribute, and experiments should be capable of testing the basic features of the NN interaction without obscuring complications. At more forward angles the character of the photon is a mixture of longitudinal and transverse so the Coulomb and electric matrix elements make big contributions and the selection of final states is more complicated.
2. The transition from I = 0 to the unbound ^1S_o with I = 1 is isovector. Therefore, besides the impulse approximation, we expect contributions from the I = 1 meson exchange currents. In this case, because of G parity conservation, the virtual photon vertex must contain a system of an even number of pions. Consequently, the one pion exchange current responsible for the long range part of the NN potential which is not visible in elastic e-d may be visible here.

The features exhibited in this simplified picture are born out by more detailed calculations as we will show below.

ii) Previous Measurements at Low Q^2

The early (and only) measurements of backward e-d* at moderate Q^2 were done in the 1960's in some of the same experiments (B3, B5) that measured the elastic $B(Q^2)$. Fig II.9 shows a schematic of a typical spectrum of scattered electrons from those measurements. Visible in the spectrum are A) the elastic peak, B) the quasi elastic peak, C) threshold for the breakup process down 2.22 MeV from the elastic peak, D) surprisingly, a small but distinct peak right at threshold with, E) a broad flat region connecting it to the quasielastic peak. This peak at inelastic threshold was immediately identified with the enhancement due to the transition to the ^1S_o final state (B10, B11).

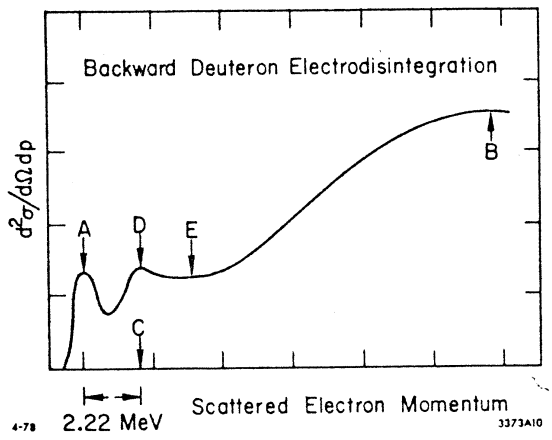

Fig. II.9. Schematic representation of a typical spectrum of electrons scattered at backward angles from deuterium in the Q^2 range 10 to 20 $1/fm^2$. The features labeled A to D are explained in the text.

iii) Early Theory - Impulse Approximation and Meson Exchange Currents

The earliest impulse approximation calculation by Jankus (G1), which did not include the deuteron D state, was in poor agreement with the old data. This situation persisted until Riska (G3) and then Hockert

et al., (G4) made a calculation for 180° scattering in the threshold region including the D state, the lowest few final state partial waves, and the simplest long range meson exchange terms. Some results from their calculation are shown in Fig. II.10. These results show two important points:

1. When the deuteron D state is properly included, the NRIA cross section to the ^1S_o state has a diffraction zero at threshold at about 12 $1/fm^2$ due to the interference between the amplitudes for scattering from the S and D states.
2. The simplest long range MEC processes completely fill in that minimum and the full cross section is in good agreement with the old data cut to $Q^2 = 10\ 1/fm^2$.

This result, and the similar success for the n-p capture problem, have been regarded as a great triumph for the MEC calculations. In fact, these are really the only two places where MEC effects can be claimed to have been seen with some confidence.

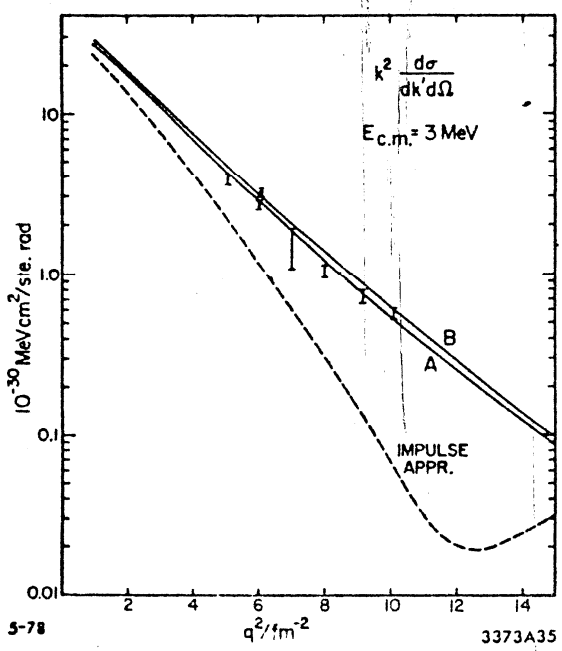

Fig. II.10. The cross section for 180° deuteron electrodisintegration near threshold, from Hockert, et al., (G4). Curve A: impulse plus π-pair MEC; Curve B: includes Δ resonance.

iv) Theoretical Questions at Larger Q^2

To indicate the kind of information we might derive from measurements of threshold electrodisintegration at larger Q^2 we can look at the calculations by Lock and Foldy (G5), Fabian and Arenhovel (G7, G8), and Sommer (G10). These authors recognized that, given that the MEC seem to be the whole effect in the diffraction minimum around 12 1/fm^2, this region would be especially sensitive to the details of those currents. They have improved on the Riska calculation by adding more partial waves and more MEC diagrams, and they give results covering the region from threshold out to several hundred MeV in relative np energy. Some diagrams for e-d* are shown in Fig. II.11. In the present state of the art, the MEC effects are calculated nonrelativistically in an ad hoc way and just added to the NRIA. Lock and Foldy did not evaluate the Coulomb or electric matrix elements since they considered only 180° scattering, but these have been calculated by Fabian and Arenhovel (G7), and they make only small contributions at 155°. Locke and Foldy included:

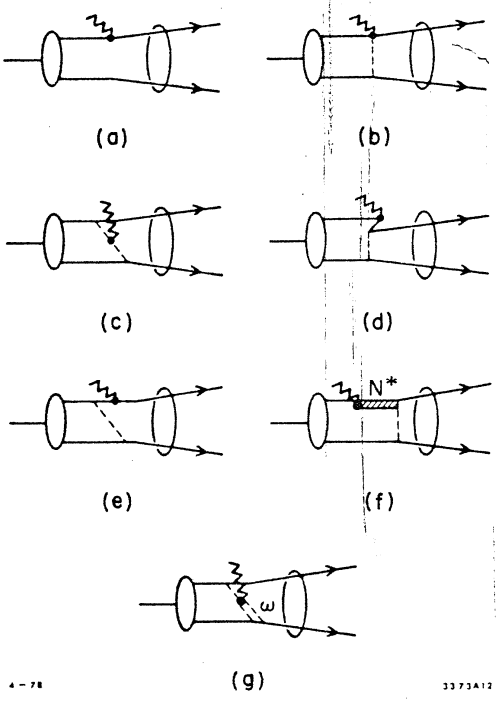

Fig. II.11. Diagrams for deuteron electrodisintegration: a) impulse approximation; b) catastrophic c) pion exchange; d) pair term which is a relativistic version of b); e) recoil term; f) isobar or rescattering term; g) heavy meson exchange.

1. NRIA transitions to many partial waves $L \geq 0$ in the final state.
2. MEC corrections to the ^1S_o final state from the catastrophic (Fig. II. 11b) or pair (II.11d) exchange term, the regular exchange term (Fig II.11c), and the isobar or so-called rescattering diagram (Fig. II.11f). Only single pion exchange was considered, i.e., no heavy mesons as in Fig. II.11g.
3. Off shell pion form factors $F_{\pi\pi}$ (k_{12}, k_{22}) in the exchange diagram.
4. A catastrophic vertex which is either pure pseudoscalar (pss) or pure pseudovector (psv). For pss coupling the vertex is proportional to the nucleon isovector form factor $F_V(Q^2)$, while for the psv they used a dipole nucleon axial vector form factor $F_A(Q^2)$ which depends on the axial mass M_A.

$$F_A(Q^2) = 1/(1+Q^2/M_A^2)^2 \qquad \text{II.2}$$

Possible values for M_A are estimated from other experiments to be in the range 0.73 to 1.05 GeV.

v) Some Predictions at Larger Q^2

The results of the Lock and Foldy calculation, some of which are shown in Figs. II.12 and II.13 bear out the basic facts of the earlier calculation by Riska, and they show important new details:

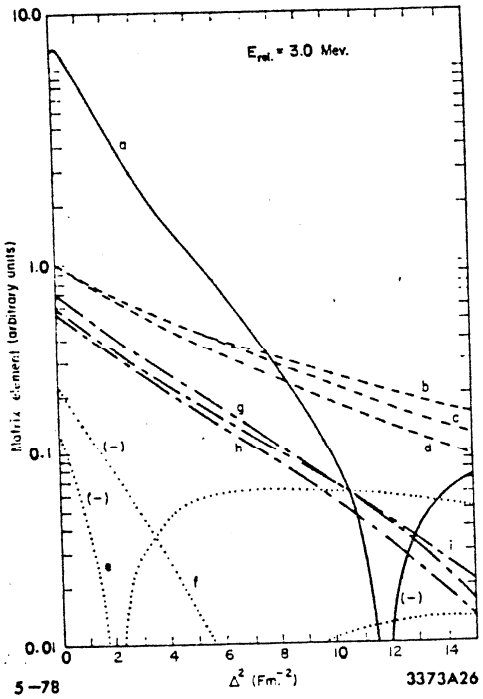

Fig. II.12. Reid hard-core matrix elements for processes contributing to deuteron electrodisintegration at 180° for E_{np} = 3.0 MeV from Lock and Foldy (G5). The curves are: a) ^1S_o impulse approximation; b-d) catastrophic with various form factors Fv and F_A; g-i) isobar term in various models; and e-f) pion exchange currents with two different F_π.

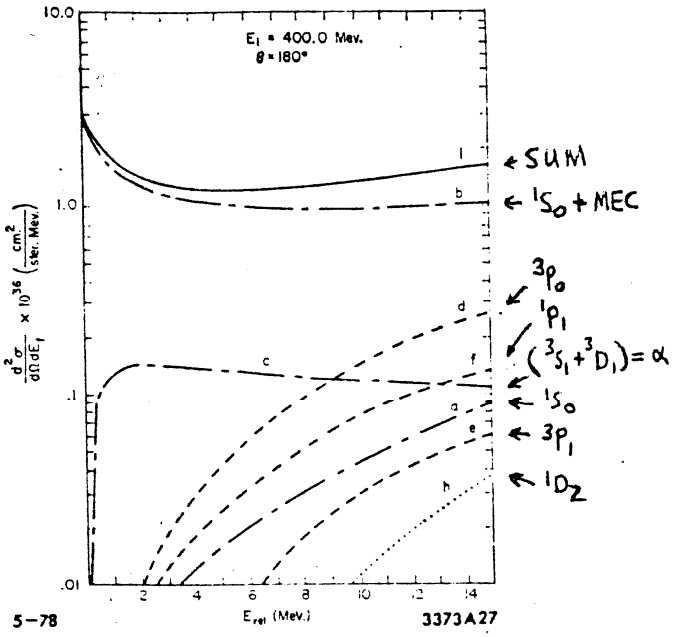

Fig. II.13. Reid hard-core double differential cross section for deuteron electrodisintegration at 180° for E_i = 400 MeV, from Lock and Foldy (G5). The final state partial cross sections are indicated.

1. The filling in of the diffraction zero in the ^1S_o state is really more of a general shift in position that is mainly due to the catastrophic or pair MEC term. The other exchange currents make much smaller contributions there.
2. In the region from threshold up to about 3 to 4 MeV relative n-p energy, the cross section is dominated by the transition to the ^1S_o state plus MEC with only about 10% from transitions

to the $^3S_1 - {}^3D_1$ (α state). The higher partial waves come in at higher energy.

3. The threshold region is sensitive to the details of the pair MEC terms, i.e., type of coupling, shape of form factors, etc.

Fig. II.14 shows the Lock and Foldy results for the full cross section for E_{np} = 3 MeV compared to the previous data. Included there are curves for the NRIA and MEC results for various choices of pion off-shell form factors, catastrophic vertex functions, and, for psv coupling, various choices of the axial mass M_A. In Fig. II.15, two of the Lock and Foldy predictions are plotted together with the results from Fabian and Arenhovel (G7, G8) extended out to 50 $1/fm^2$. Fig. II.16 shows the prediction by Sommer (G10) for the same kinematic region as Fig. II.15. From these figures we see again, as with the elastic form factor, the general result that the exchange currents drastically alter the shape and position of the

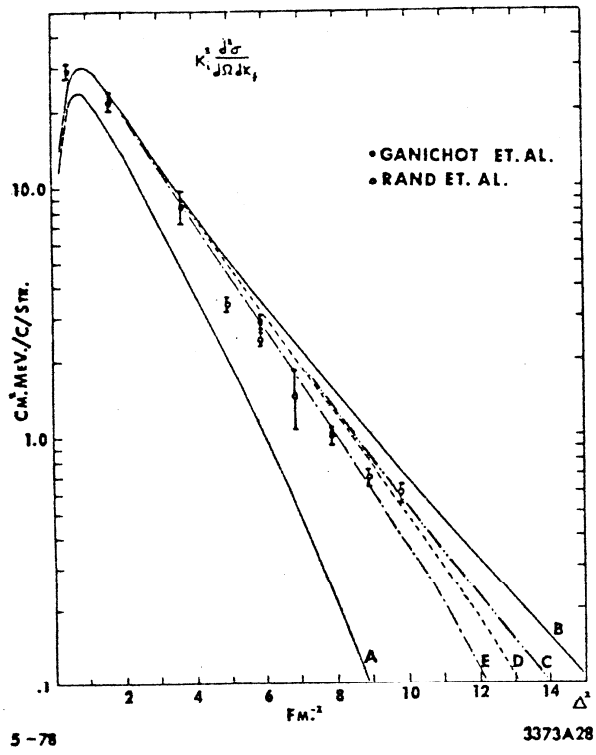

Fig. II.14. Deuteron electrodisintegration cross section near threshold for back-scattered electrons at low Q^2, from Lock and Foldy (G5). The curve A is the impulse cross section to the final $^1S_0$ state. The curves B-E are the impulse plus MEC contributions with various assumptions for F_V, F_A and $F_{\pi\pi}$. The data are from Refs. (B3) and (B5).

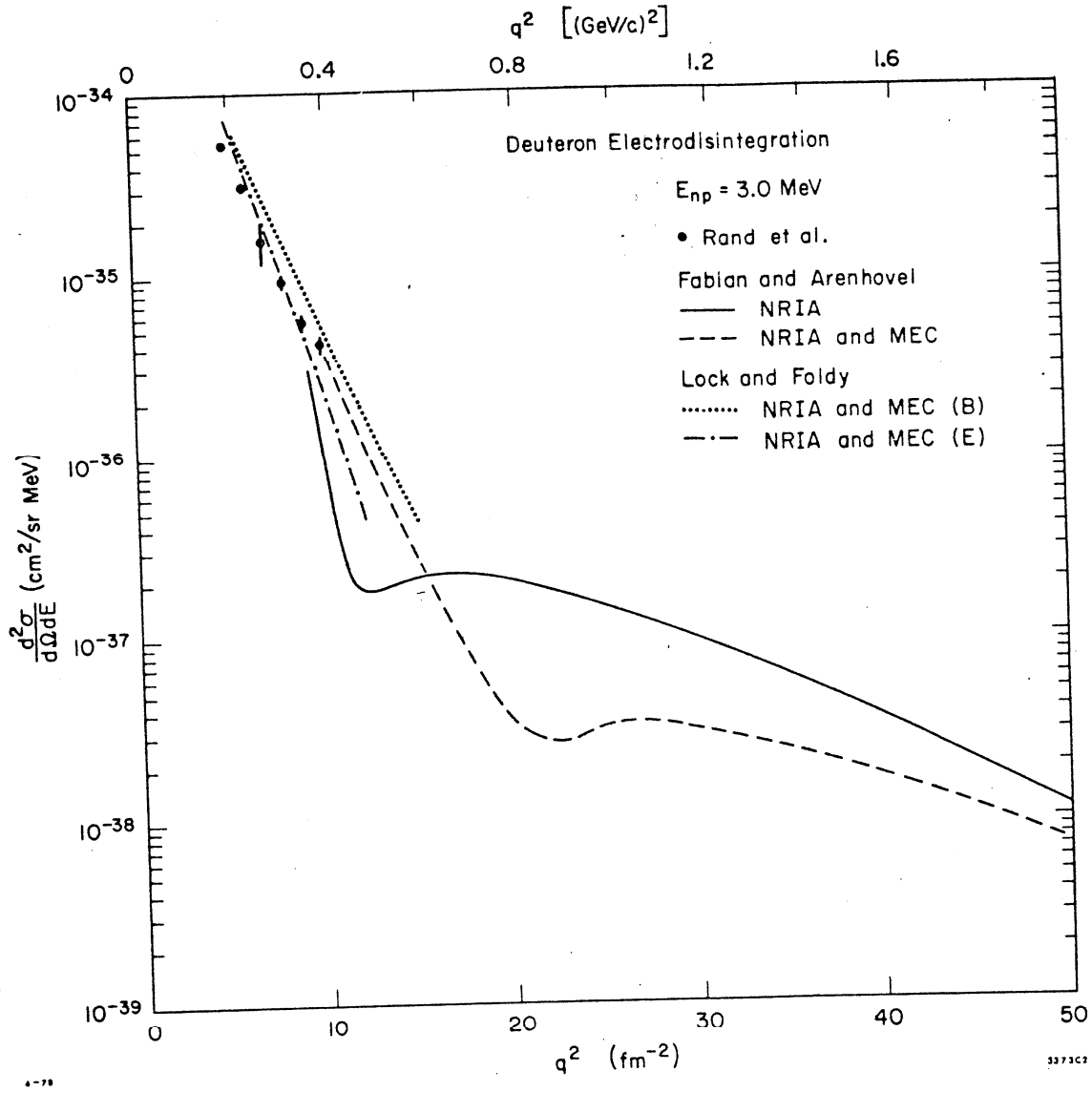

Fig. II.15. Deuteron electrodisintegration cross sections near threshold for back-scattered electrons at high Q^2. The curves labeled (B) and (E) from Lock and Foldy represent the range of predictions for the impulse plus MEC calculations for 180° scattering at low Q^2. The two curves extending to higher Q^2, with and without MEC contributions, are from Fabian and Arenhovel (G7, G8) for scattering at 155°. The data are from Ref. (B5).

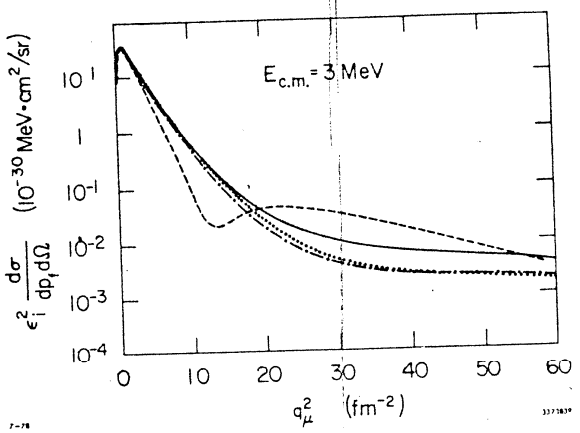

Fig. II.16. Deuteron electrodisintegration cross section at 180° from Sommer (G10) containing all transitions to final states with $J \geq 2$ for E_{np} = 3 MeV. Dashed line: NRIA, dotted line: NRIA + MEC, dashed-dotted line: NRIA + MEC + Δ, all with RSC potential (6.47% D state), full line: same as dotted line except with a deTourelli-Sprung potential (4.5% D state).

diffraction features. The shapes of the various theoretical predictions are not quite the same, reflecting the sensitivities to differences in the input to the calculations. Notice in particular the difference between the solid curve and the dotted curve in Fig II.16 which indicates the sensitivity to the percent D state at large Q^2.

vi) Possible Experimental Results

Our proposed experiment will measure the inelastic cross section at threshold at forward and backward angles with resolution of several MeV and statistical errors at the level of 5 percent or better over the entire Q^2 region 12 to 50 1/fm^2 (0.4 to 2.0 (GeV/c)^2. The details of the run plan are described in Section III.B and in Table IV. We will easily distinguish between the various predictions with and without meson exchange currents displayed in Figs. II.14, II.15, and II.16. The measurement at lower Q^2 will be a valuable check on the previous limited experimental results, while the high Q^2 data will extend the knowledge of the threshold inelastic cross section down by over two orders of magnitude and out a factor of five in Q^2 over the previous experiments. This data will rival the elastic data in its importance for distinguishing possible meson exchange and isobar effects from the shapes of the diffraction features.

vii) Summary of Motivation for Measuring Backward Threshold Inelastic Scattering in the Range $0.4 < Q^2 < 2$ (GeV/c)^2

As is the case with the isoscalar structure functions in elastic e-d, the largest contributions to the MEC processes in inelastic e-d* comes from the so-called catastrophic or pair terms, Fig. II.11b and II.11d. F. Gross has argued (E5), similarly to the elastic case, that these pair terms are not really a true MEC but are more properly treated as part of the total relativistic wave function of the n-p-d vertex. Therefore, one can regard the purpose of higher Q^2 threshold e-d* measurements as follows:

1. To the extent that we get good agreement with the data using the NRIA plus MEC corrections we can test the details of the isovector MEC processes; i.e., form factors, couplings, etc., to complement the study of isoscalar MEC in the elastic form factor $B(Q^2)$. For example, under the assumption that processes other than the catastrophic term are all much smaller or can be calculated, and that the catastrophic coupling is psv, one can determine the nucleon axial vector form factor $F_A(Q^2)$ over a range of Q^2, and then perhaps deduce the axial mass and maybe even decide whether the axial vector form factor is dipole or not.
2. If we don't get good agreement using the NRIA plus ad hoc MEC corrections, the new data may indicate that a more systematic approach is needed, such as that suggested by Gross. We would expect many approximations of the NRIA theory to become inadequate with increased Q^2, say beyond 15 to 20 1/fm^2. Data at larger Q^2 would

be the place to eventually test a more complete theory including all MEC effects in a self consistent relativistic calculation.

This unexplored region in threshold inelastic e-d* was cited in a recent DCE/NSF sponsored study (K5) as one of THE important electron experiments for medium energy nuclear-structure physics.

C. Quasi Elastic Scattering $0.4 \leq Q^2 \leq 2$ $(GeV/c)^2$

In the third portion of the proposed experiment we will extend the measurement of inelastic single arm electron scattering over the entire quasi elastic peak in the Q^2 region 0.4 to 2 $(GeV/c)^2$. The kinematic regions to be covered are explained in more detail in Section III.B and Fig. III.3. The aim of this measurement is to get the best data possible over the entire quasi elastic region (statistical error less than 5% per 5 MeV bin in E_f). Similar data has been obtained in previous experiments at CEA (L1-L3) and DESY (L4) in the late 1960's, mainly for the purpose of extracting neutron cross sections. Data of sufficient accuracy was obtained to determine peak areas or peak heights, but the range of kinematics covered was more limited and the resolution and the statistical errors were generally worse than we can easily achieve.

We are primarily interested in the quasi elastic data as an extension of the threshold inelastic data to higher missing mass. We want to study the detailed shape of the cross section from inelastic threshold where a few partial waves and possible MEC terms make up most of the cross section, over the peak, where many partial waves contribute, right up to the resonance region. We can compare this high statistics data to the inelastic calculations including many partial waves, like those of Fabian and Arenhovel (G7) and Sommer (G10) and to others including excitation of nucleon resonances. We are especially interested

in the cross section on the upper side of the quasi elastic peak, where, as near the inelastic threshold, the high momentum components of the deuteron wave functions are most important. There is some evidence in the ^{3}He and ^{4}He data at lower Q^2 (L5, L6) that there is an excess of cross section in that region which cannot be attributed to quasi elastic scattering from individual nucleons or to scattering from the Fermi smeared nucleon resonances. A careful measurement in the region between the quasi elastic peak and the resonances in the deuteron may also show an excess cross section, which is probably due to meson exchange processes similar to those which enhance the cross section at inelastic threshold.

With this experiment we would be making two new contributions in an area that has been looked at before: a) we would obtain data of sufficient statistical accuracy to make a detailed comparison with the theory over the kinematic region in Fig. III.3 at the level of 5% or better, and b) we would make measurements at forward and backward angles in the same apparatus covering the same regions in Q^2 and W from which we could extract longitudinal and transverse cross sections. A careful measurement of $R = \sigma_L/\sigma_T$ in the quasi elastic region at Q^2 0.4 to 2 $(GeV/c)^2$ has not been done previously. This could be especially important for understanding the source of any possible excess cross section at large missing mass.

D. Elastic and Inelastic e-d at Large Q^2: $Q^2 > 1$ (GeV/c)^2 - Quarks in the Deuteron

i) The Experiment at Large Q^2

For the fourth portion of the proposed experiment we will measure single arm inelastic scattering cross sections near threshold at 155° out to the largest Q^2 possible in a reasonable running time, about $Q^2 = 5$ (GeV/c)^2. This will cover the region in Q^2 where the internal structure of the nucleons and scaling may begin to appear. The elastic measurement, limited to $Q^2 \leq 2$ (GeV/c)^2 by counting rates, will just barely extend into the scaling region, and will be better described by the nuclear-physics models and perhaps by some of the preasymptotic or approach-to-scaling predictions.

Some of the most convincing evidence for the quark structure of nucleons comes from deep inelastic lepton scattering (ν, $Q^2 > 1$ GeV^2) from hydrogen and deuterium at large missing mass W (W > 2 GeV/c) where the structure functions exhibit the now famous scaling behavior characteristic of scattering from pointlike quark-partons. The region of deep inelastic scattering from the nucleons near the elastic kinematic limit has also been an especially rich area (A2, H1-H7, J3). We are interested in extending this study to scattering from light nuclei in two transition regions: a) the transition with increased Q^2 from nuclear to quark physics, and b) the transition with increased missing mass W from elastic to deep inelastic scattering. In our previous experiment we measured $A(Q^2)$ (A1) and νW_2 (A2) in these transition regions. Now we turn our attention to the backward angle structure functions $B(Q^2)$ and $2MW_1$ to learn more details about the interplay between nuclear and nucleon structure.

ii) Basic Ideas About the Quark Structure of the Deuteron

How is the quark structure of the nucleons related to the nuclear (deuteron) structure functions in the regions in Q^2 and W to be covered by our experiments?

We can understand the quark model predictions for nuclear structure functions in this region in the following simplified picture, illustrated schematically in Fig. II.17. The underlying idea of the standard dogma is that the constituents are pointlike, and that the basic interactions are (nearly) scale invariant. The ideas sketched in Fig. II.17 and described briefly below are mainly those of the Dimensional Scaling Quark Model (DSQM) (J1) and the Constituent Interchange Model (CIM) (J2). They are the work of many people in recent years and grew out of a vast amount of experimental evidence from deep inelastic lepton scattering and high transverse momentum hadron reactions that nucleons are somehow "made of" pointlike quark-partons.

a. Basic Ideas About Quarks - Elastic Scattering

For the case of elastic electron scattering at very large Q^2 off a nucleus of momentum p, the virtual photon can be pictured to connect to one of the constituent point-like quarks, Fig. II.17a. Then by successive interactions (or perhaps also quark rearrangement) the momentum transfer q must be shared roughly equally with the rest of the quarks, leaving the nucleus intact and recoiling with momentum (p + q).

The typical Fermi momentum of a quark bound in a hadron is 300 to 500 MeV/c, and the binding affects the shape of the structure functions in the preasymptotic region. However, at very large Q^2 the quarks are pictured to be essentially free when they are struck by the virtual photon, and there

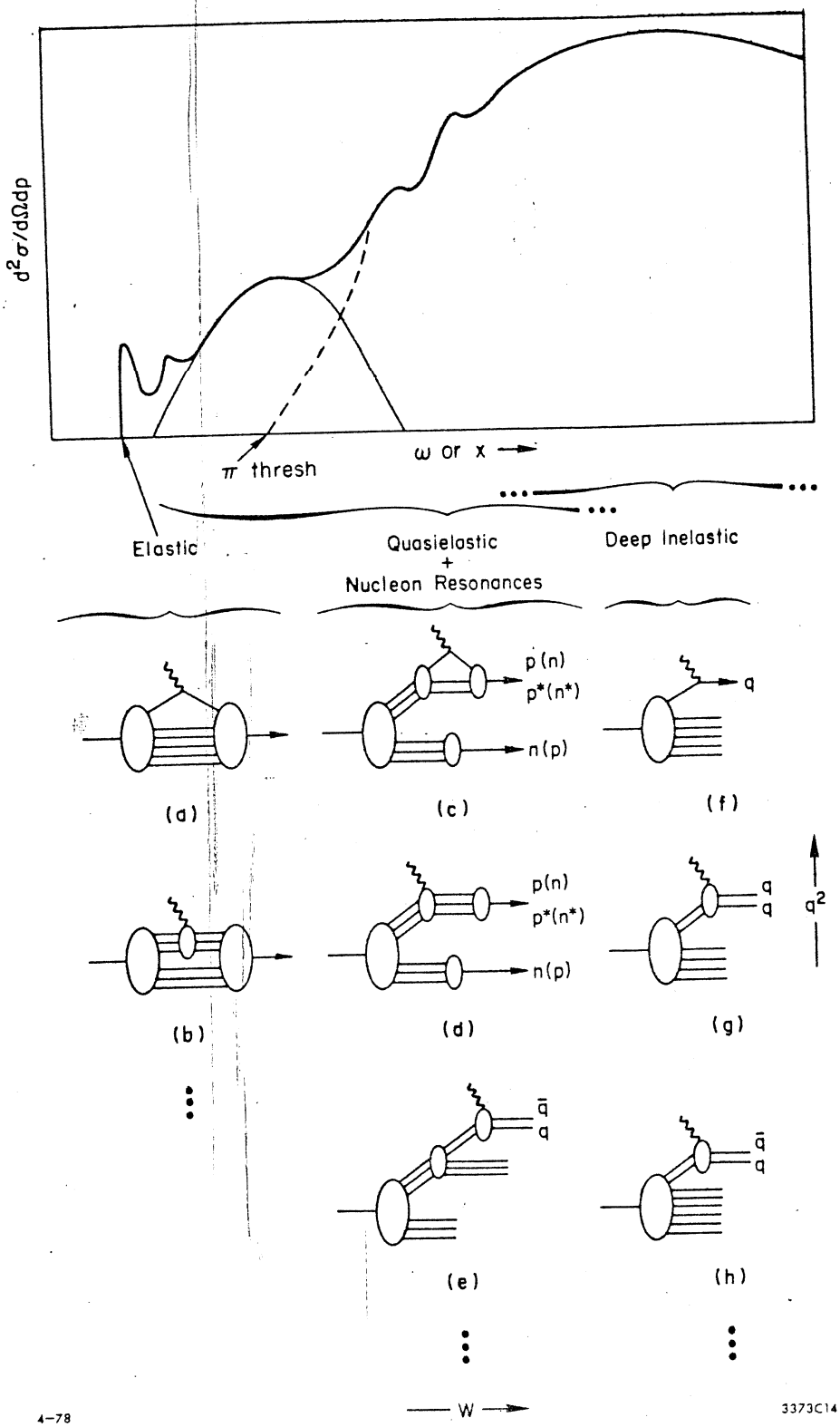

Fig. II.17. Schematic picture of electron deuteron cross sections from the elastic to the deep inelastic region. Indicated below are diagrams (explained in the text) sketched in the spirit of the dimensional scaling quark model (J3) including possible multiquark diagrams for the preasymptotic region following the suggestion by Schmidt and Blankenbecler (J4).

is little effect on the shape of the structure functions from initial or final state interactions of the quarks with each other. One can picture the momentum transfer propagating through a chain of gluons as occuring either before or after the photon interaction.

In some recent work, Brodsky and Chertok (J3), following the work of Brodsky and Farrar (J1), have applied the ideas of quark dimensional scaling and the Constituent Interchange Model (J2) to a study of nucleon and nuclear form factors. They show how the shape of hadron form factors is determined by the degree of compositness of the object, and that the same target can reveal different degrees of structure depending on the Q^2 with which it is probed. At truly asymptotic Q^2 the elastic form factors fall with powers of Q^2 determined by the number of constituents (quarks) in the target by

$$F_H = \sqrt{A} \sim (1/Q^2)^{n-1} \qquad \text{II.3}$$

Eq. II.3 contains a factor of $1/Q^2$ for each quark which changes momentum. The fact that the quarks are pointlike means that there is no mass anywhere in the theory to set the scale of distance in the basic photon-quark or quark-quark interaction.

What is the evidence to date that the Dimensional Scaling Quark model works for the deuteron? Some of the DSQM predictions are compared

to experiment in Figs. II.18 and II.19. Since the DSQM predicts only the shape of the structure functions and not the absolute normalization, we compare the shapes by displaying the ratio F_{exp}/F_{DSQM}. The value of Q^2 where the ratio becomes a constant depends on whether we compare to the truly asymptotic predictions of Eq. II.3 as in Fig. II.18, or to the preasymptotic predictions with binding corrections, one of which is shown in Fig. II.19.

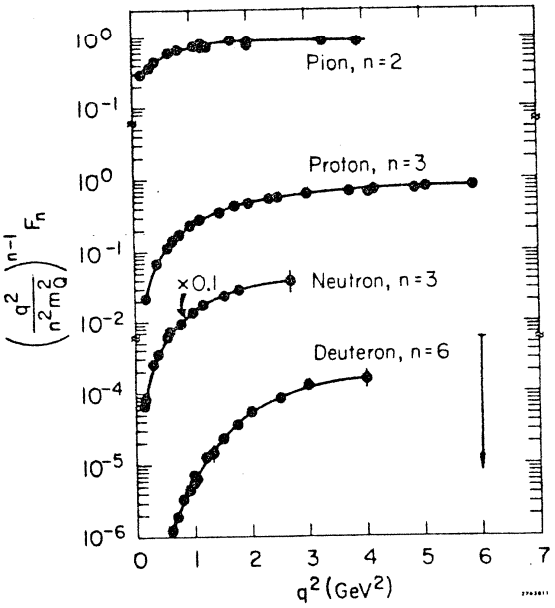

Fig. II.18. Elastic electromagnetic form factors of hadrons for large spacelike Q^2 divided by the dimensional scaling quark model from Brodsky and Chertok (J3). The curves simply connect the data points. The neutron data have been multiplied by 0.1.

The ratio F_{exp}/F_{DSQM} using Eq. II.3 approaches a constant somewhere above $Q^2 = 4$ (GeV/c)^2, while using the preasymptotic models, it does so in the region

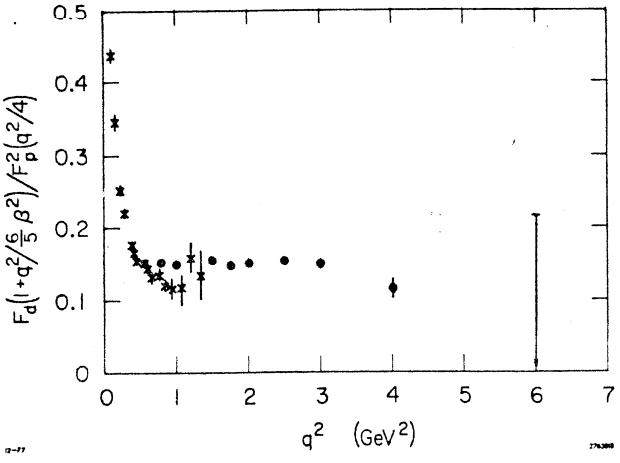

Fig. II.19. The deuteron form factor $F_d = \sqrt{A}$ divided by the quark interchange prediction, from Brodsky and Chertok (J3). The data are from Ref. (A1) and other experiments.

1 to 2 $(GeV/c)^2$. We conclude from this evidence that the quark structure is beginning to appear in $A(Q^2)$ in the Q^2 region 1 to 4 $(GeV/c)^2$.

Another way to view the preasymptotic region, suggested recently by Schmidt and Blankenbecler (J4, J5), is to consider that the photon may connect to groups of quarks (or perhaps also to quark-antiquark pairs from the $q\bar{q}$ sea) rather than to single quarks only. This is a natural point of view since the Fermi motion, which dominates the structure in the preasymptotic region, is due to the presence of the other quarks. In their theory the amplitude for the photon coupling to groups of quarks, as in Fig. II.17b is proportional to

$$F \sim A_n(x)\, F_n^2(Q^2)\, (1-x)^{n_{spec}-1} \qquad \text{II.4}$$

where $x = Q^2/2M\nu$ is the scaling variable and n_{spec} is the number of spectator quarks and M is the nucleon mass. The factor $(1-x)^{n_{spec}-1}$ reflects the chance for finding n quarks in the target at a particular x. The factor $F_n(Q^2)$ is the form factor for that subgroup of n quarks and A_n is a normalization parameter. The objects with three quarks in a nuclear target, as in Fig. II.17b, might be identified with the nucleons, and the form factors $F_n(Q^2)$ would be the usual nucleon form factors, while the factors $A_n(1-x)^{n_{spec}-1}$ would then be related to the usual nuclear wave functions. Schmidt and Blankenbecler do not consider either the spins of the quarks or of the nucleons, thus they only discuss scalar form factors. The primary question from the point of view of this experiment at high Q^2 is: What determines the angular distribution of the elastically scattered electrons; i.e., what can we expect for $B(Q^2)$ or the ratio B/A as we move from low to high Q^2?

In the preasymptotic region of Q^2, the ratio B/A, in the nuclear physics language, will be governed by the nuclear wave functions and nucleon form factors, plus possible MEC or IC effects. We have already described in Section II.A what we learn from $B(Q^2)$ in these models. On the other hand, Blankenbecler and Schmidt would say that the angular distribution in the approach-to-scaling region will be determined by the distribution from all the various possible subprocesses of scattering from quarks or groups of quarks in proportion to the contribution each makes to the full cross section at a particular angle and Q^2. An extension of their work for the deuteron elastic structure functions to include the deuteron spin has been done by Fernandez-Pacheco et al., (E3). Their results for $B(Q^2)$ are shown in Fig. II.5 and compared there with some nuclear-physics calculations.

As the preasymptotic region merges with the truly asymptotic regime at large Q^2 (how large is large??) the scattering from the individual spin 1/2 quarks should dominate. For that region Brodsky and Chertok (J3) predict

$$B(Q^2) \to \frac{Q^2}{2M} A(Q^2) \quad . \qquad \text{II.5}$$

A recent paper by Vainshtein and Zakharov (VZ) (J9) has raised another interesting point. They consider diagrams like Fig. II.17a and point out that the relative size of the longitudinal to transverse elastic cross sections, $\sigma_L^{el}/\sigma_T^{el}$, depends in detail on the way the photon and gluons share the momentum transfer q among the quarks. In a theory with vector gluons and spin 1/2 quarks, they predict that for a target of n quarks:

$$\frac{\sigma_L^{el}}{\sigma_T^{el}} \gg 1 \text{ for n even} \qquad (Q^2 \to \infty) \qquad \text{II.6}$$

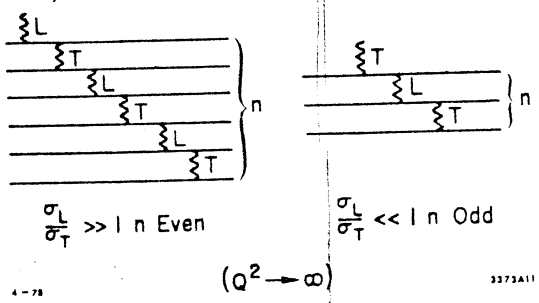

Fig. II.20. Quark diagrams for elastic form factors for three-quark and six-quark hadrons, after Vainshtein and Zakharov (J9). The symbols L and T indicate longitudinal and transverse photons and gluons.

$$\frac{\sigma_L^{el}}{\sigma_T^{el}} << 1 \text{ for n odd} \qquad (Q^2 \to \infty) \qquad \text{II.7}$$

They get this result from two effects:

1. The interaction of a transversely polarized gluon attached to the lowest quark line in Fig. II.20 is $(Q^2)^{\frac{1}{2}}$ times larger than that of a longitudinally polarized gluon.
2. For Compton scattering (photon-gluon or gluon-gluon) the amplitude is largest when one gluon (photon) is longitudinal and the other is transverse. If both are polarized the same way there is an extra damping factor of $(Q^2)^{-\frac{1}{2}}$.

Thus the dominating contribution comes when the bottom gluon is transverse and the rest are alternately longitudinal and transverse as illustrated in Fig. II.20. The result is also true for different permutations of quarks and gluons not necessarily arranged in a direct chain. (These arguments are similar to those used by Farrar and Jackson (H4) to predict the ratio of neutron to proton cross section near $x = 1$, $\sigma_n/\sigma_p = 3/7$.)

Therefore, contrary to the Brodsky-Chertok prediction in Eq. II.5 where the angular dependence at asymptotic Q^2 comes directly from the

elementary scattering on the constituents, Vainshtein and Zakharov (J9) suggest that the dynamics of the quark-gluon interaction responsible for keeping the target intact also strongly affects the angular distribution. A similar argument should apply for the ratio $R = \sigma_L/\sigma_T$ near $x = 1$ in the inelastic region where the target is "almost" left intact.

b. Basic Ideas About Quarks - Inelastic Scattering

For inelastic scattering, the virtual photon can destroy the nucleus in a number of ways. In the threshold region of W, say a few MeV from break-up, the dominant mechanism is quasi elastic scattering from the bound nucleons as in Fig. II.17c or II.17d. Another mechanism might be scattering from the exchange currents as discussed in Section II.B. For larger energy loss, pions can be produced in resonant (Fig II.17c or II.17d) or nonresonant (Fig. II.17e) scattering from the nucleons, and at large W in the deep inelastic region many pions can be produced by many mechanisms (Figs. II.18f, g, h, etc.).

In our simplified picture in Fig. II.17 we illustrate the continuous progression through the transition regions in Q^2 and W. As W decreases we move from a completely incoherent sum of scattering from individual quarks or subgroups of quarks in the deep inelastic on the right to the completely coherent elastic scattering on the left. As the Q^2 increases we expect the cross section to be more and more dominated by contributions from the diagrams at the top of the columns in Fig II.17. Also, the quasi elastic and resonance regions overlap with each other and with the deep inelastic region. As Q^2 increases they squeeze down into the left hand side of the figure versus the scaling variable x or ω' as the resonances and quasi elastic peaks sink into the nonresonant background (H3). At truly asymptotic Q^2 the entire inelastic region is dominated by the diagram in Fig. II.17f and the elastic by Fig. II.17a.

The primary question for our proposed experiments is: What can we learn from angular distributions of electrons scattered inelastically from nuclear targets in the transition regions of Q^2 and W? In the context of the schematic quark picture presented above, we expect the angular distribution of the full cross section to be a reflection of the angular distributions from the various subprocesses in proportion to the contribution each makes at a given Q^2 and W. For example, in the quasi elastic and resonance regions of W and in the preasymptotic region of Q^2, we expect $R = \sigma_L/\sigma_T$ to partially depend on the structure functions of the nucleons and the nucleon resonances, smeared by the Fermi motion from nuclear binding. In the language of the Blankenbecler-Schmidt theory, we would be learning about the factors in Eq. II.4. Their results for the νW_2 function are compared with the data in Fig II.21. There does not yet exist a comparable calculation for $2MW_1$.

In the deep inelastic region at asymptotic Q^2 where the cross section is mostly due to the incoherent sum of scatterings from individual spin 1/2 quarks, the transverse cross section dominates. The ratio of the longitudinal to transverse cross sections from the spin 1/2 quarks behaves as

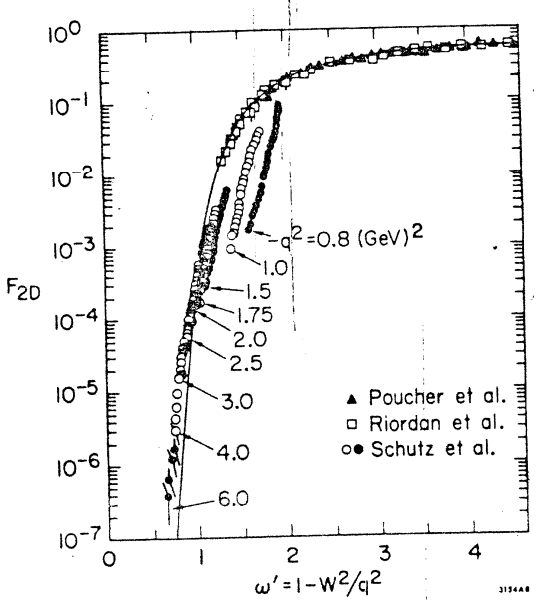

Fig. II.21. The deuteron inelastic structure function $F_{2D} = \nu W_2$. The data are from Refs. (A2), (B8, B9). The curve is from the quark model for the approach-to-scaling region by Schmidt and Blankenbecler (J4).

$$R = \sigma_L/\sigma_T \to 0 \qquad \text{II.8}$$

(Callen-Gross relation (J12)). The present experimental value for R from e-p (e-d) scattering (B8) is 0.138 ± 0.065 (0.175 ± 0.060), roughly independent of Q^2 and W. This is one of the primary pieces of evidence that the quarks are pointlike and spin 1/2.

iii) Elastic-Inelastic Connection

Brodsky and Chertok have generalized the Bloom-Gilman (H3) argument to nuclei and suggest that there must be a smooth connection from the inelastic near $x = 1$ ($x_d = 2$) to the elastic at high Q^2 (exclusive-inclusive connection) which we illustrated schematically as the progression from right to left in Fig. II.17. They predict:

$$\frac{B}{A} \to \frac{2W_1}{W_2}\Bigg|_{x_d = 2} \qquad \text{II.9}$$

iv) Six-Quark Coupling Calculations and the Possibility of Hidden Color in the Deuteron

There are several other recent developments in the direction of looking at the deuteron as a system of quarks. Matveev and Sorba have done a group theory study of the possible coupling schemes for six colored quarks (J6, J7). They have suggested that the deuteron may "tunnel" into a six-quark state with hidden color with as much as 5.6% probability (J7). They support their argument partly with evidence from the $A(Q^2)$ data at large Q^2. In a recent preprint, A. P. Kobushkin has also made a six-quark coupling calculation (J8). Fixing the 2% probability for the six-quark state from the magnetic moment

anomaly, he calculates the elastic structure functions and suggest that may be the place to look for the six-quark state. His results are displayed in Figs. II.22 and II.23.

C. DeTar has done a study of the two nucleon interaction in the context of the MIT bag model (J10). He used a static cavity approximation and looked at the system of six colored quarks with the quantum numbers of

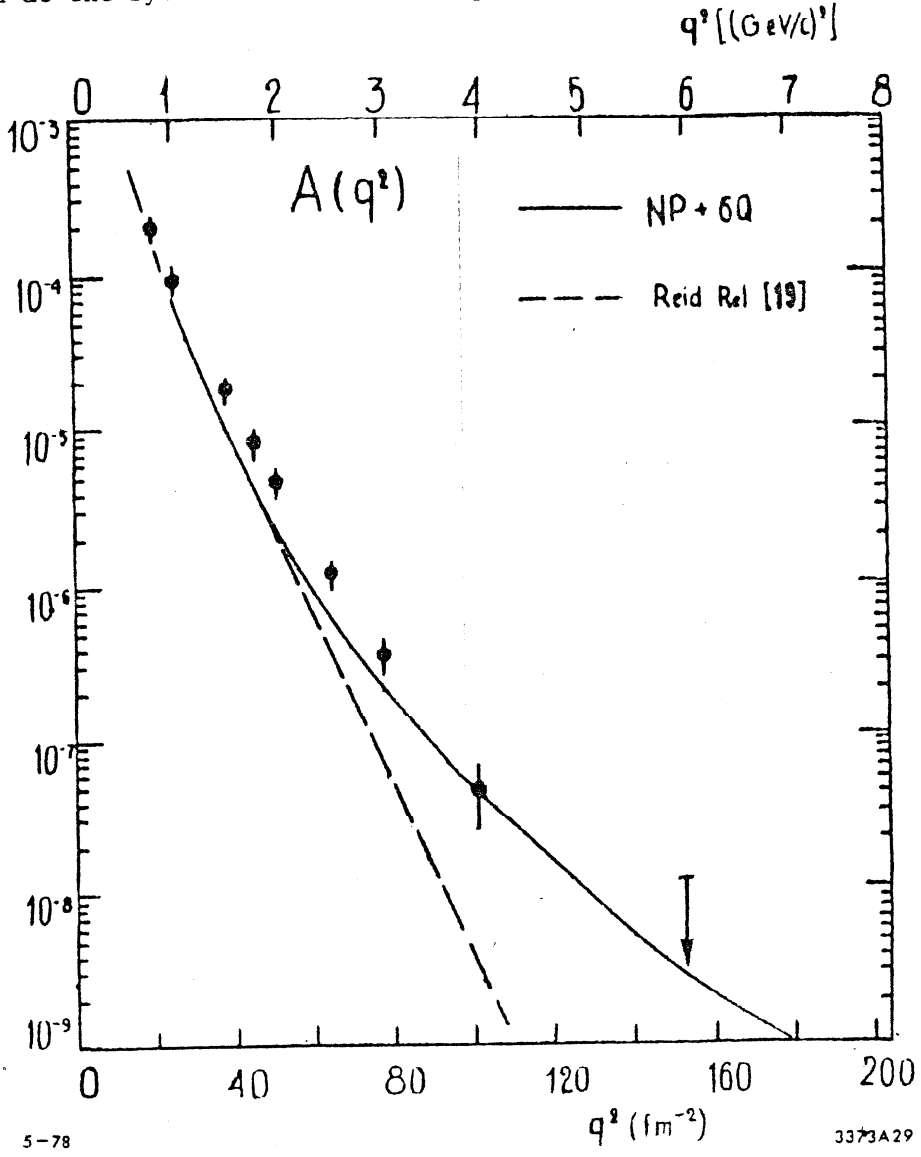

Fig. II.22. The deuteron form factor $A(Q^2)$ assuming 2% probability for the six-quark state, from Kobushkin (J8).

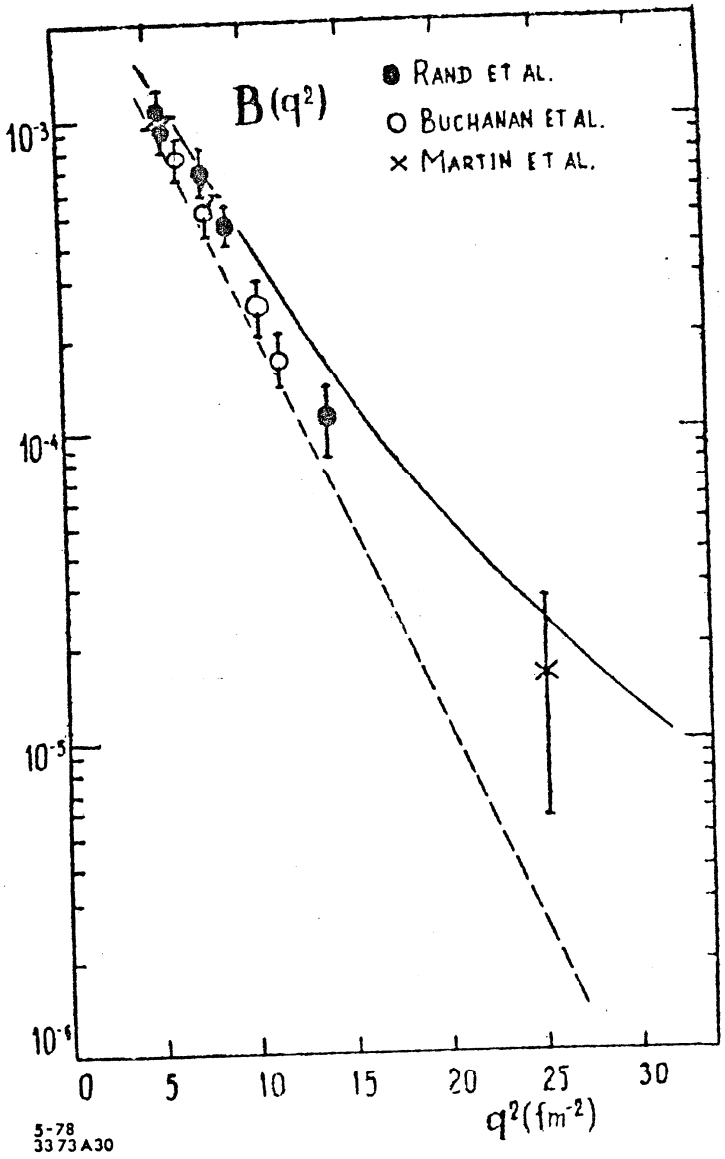

Fig. II.23. The deuteron form factor $B(Q^2)$ assuming 2% probability for the six-quark state, from Kobushkin (J8).

the deuteron. The bag was allowed to adiabatically change shape from the single bag with six quarks to two nucleon bags of three quarks each (see Fig. II.24). In the short and intermediate ranges of interaction that he studied, the model exhibited a soft short range repulsive core due to color-magnetic gluon interaction and a strong attraction in intermediate range due to color-electric interaction (see Fig. II.25).

In their present form these models with quark states in the deuteron have too many simplifications (static cavity, no nucleon momentum dependence, guesses at percent six-quark state, etc.) to give a realistic description of the actual deuteron, but this work does indicate the direction that nuclear physics at short distances is taking. In future years when people investigate the NN interaction at distances inside 1/2 fermi,

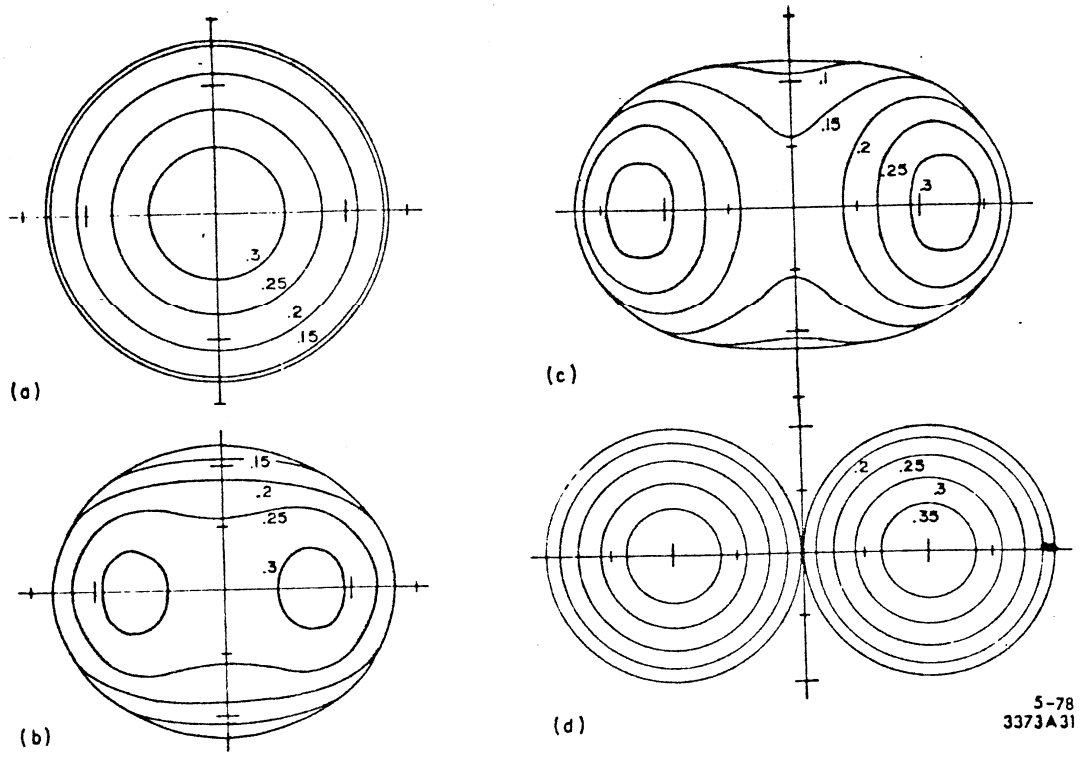

Fig. II.24 (above). Curves of equal baryon density (baryons/fm^3) in a longitudinal cross section of the six-quark MIT bag model at various constrained separations: a) $\delta = 0$; b) $\delta = 0.8$ fm, minimum energy; c) $\delta = 1.4$ fm; d) two noninteracting nucleons for comparison, from DeTar (J10). Scale markers are in 0.5 fm.

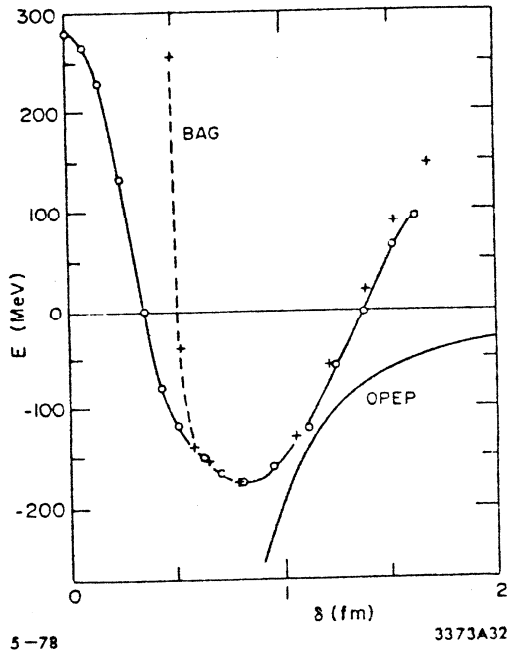

Fig. II.25 (left). Two-nucleon interaction energy vs. the constrained baryonic quadrupole moment Q (fm^2) for the six-quark system with $I = 0$, $S = 1$, $|m_S| = 1$ in the MIT bag model (solid line with circles). The one pion exchange potential is shown for comparison, from DeTar (J10).

they most surely will be discussing the quark structure of the system. To make progress in this area what is needed are measurements of the electromagnetic currents at large Q^2, which we are proposing to provide.

v) Some Predictions at Large Q^2

Since there are no direct calculations of $2MW_1$, we have used our previous data for νW_2 and have made the following rough estimates above $Q^2 = 2$ for purposes of estimating counting rates and illustrating the range of predictions:

1. $R \to$ small: We express the ratio $2MW_1/\nu W_2$ in terms of R using:

$$\frac{2W_1}{W_2} = \frac{Q^2}{2M^2}\left(\frac{1 - 4M^2/Q^2}{1 + R}\right) \qquad \text{II.10}$$

Then assuming $R = 0.18$, we predict $2MW_1$. This is equivalent to assuming the angular distribution from the deep inelastic right up to inelastic threshold is determined by the elementary scattering from spin 1/2 quarks, as suggested by Brodsky and Chertok (J3). This prediction contradicts the suggestion by Vainshtein and Zakharov (J9).

2. $R \to$ large: We used the elastic-inelastic connection of Eq. II.9 and the values for $A(Q^2)$ and νW_2 from experiment (A2) together with the range of values for $B(Q^2)$ covered by the models in Fig. II.4 to predict $2MW_1$. This is equivalent to assuming that the angular distribution is affected by the cooperative behavior of the quarks and

that R is 10 or 100 near the inelastic threshold, which agrees with the VZ argument.

These two estimates for $2MW_1$ for Q^2 = 2 to 6 $(GeV/c)^2$ are shown in Fig II.26 together with the previous data at large Q^2 and large W. Also shown there is the prediction at lower Q^2 from the NRIA plus MEC calculation by Fabian and Arenhovel (FA) G7), and the proposed limit to be set by this experiment.

vi) Possible Experimental Results

The high Q^2 threshold inelastic portion of this experiment is described in Section III.B and Table VI. The maximum value of Q^2 at which a signal may be seen is determined by the rate at which $2MW_1$ falls with increased Q^2. The limit of sensitivity at 155° with beam currents of 100 mA peak at 180 pps for five events in 100 hours corresponds to $2MW_1$ at the level of 2 to 6 $\times 10^{-6}$ in the Q^2 range 2 to 5 $(GeV/c)^2$. This corresponds to a limiting cross section of approximately $d\sigma/d\Omega dE = 4 \times 10^{-42} cm^2/sr/MeV$. (See Fig. II.26). We plan to use the requested hours for high energy inelastic single arm running to push the measurement to that level of sensitivity at whatever Q^2 that occurs. At this level we will be able to distinguish whether the Brodsky-Chertok prediction based on the assumption that R is small is true, or whether R at threshold is in fact as large as 10 or 100 . The proposed high energy measurement will extend the knowledge of $2MW_1$ down by over two orders of magnitude below the previous SLAC data. It will yield a series of spectra which may tend to a universal "scaling" curve when plotted versus ω', perhaps indicating that the quark structure of the nucleons is determining the shape of the nuclear structure function in that region.

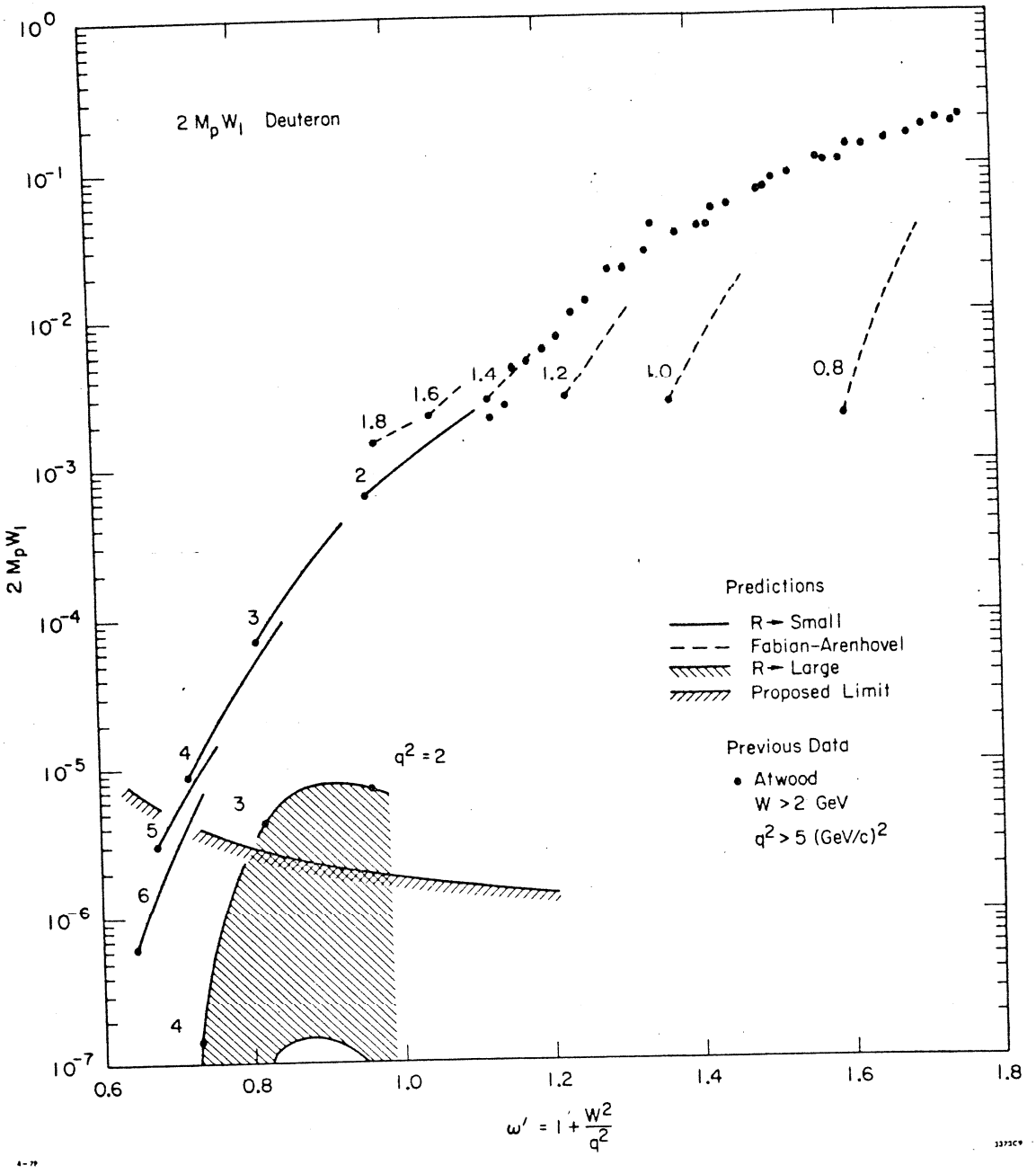

Fig. II.26. Overview of the range of predictions for the deuteron structure function $2MW_1$. The dotted curves represent the nuclear physics prediction of Fabian and Arenhovel (G7, G8) at lower Q^2 with impulse and MEC contributions corresponding to the dotted curve in Fig. II.14. The curves labeled R→ small and the range labeled R→ large are the high Q^2 predictions explained in the text. The curves indicated the possible shape of the spectra for fixed E_o with the location of the inelastic threshold indicated by the dots. The numbers beside are the Q^2 values at the elastic peak. The data are from Ref. (B6).

vii) Summary of Motivation for Backward Angle Scattering at Large Q^2

The inelastic data spanning the transition regions in Q^2 and W described above, taken together with the elastic data for $B(Q^2)$, would provide much information on such questions as:

1. Where does the nuclear physics NRIA break down? At what Q^2 do we need a relativistic treatment of threshold electrodisintegration?
2. Do meson exchange or isobar currents play a large role in threshold inelastic scattering at large Q^2?
3. Is there a smooth connection between elastic and inelastic structure functions as predicted by Eq. II.9. If not, does the breakdown depend on Q^2?
4. At what Q^2 do we reach the asymptotic region for $2MW_1$? Is it near $Q^2 = 2\ (GeV/c)^2$ as for νW_2?
5. What is the value of R in the threshold region?
6. Can we deduce the relative contributions of possible subprocesses in the preasymptotic region? If so, what is the angular distribution from the dominant subprocesses.
7. How does the dynamics of the sharing of the momentum among the quarks affect the angular distributions? Can we see evidence in support of the model of nucleons with spin 1/2 quarks and vector gluons?
8. Can we understand the function $B(Q^2)$ in the preasymptotic region using the same forms for binding corrections that seemed to work so well for $A(Q^2)$?

9. Can we use the new data to guide our thinking as we try to make the connection between the traditional nuclear physics description and the quark models? Where do the meson exchange and isobar configurations fit in the quark picture in nuclei? In what domain of Q^2 or W do the nuclear and quark descriptions do well, overlap and then eventually break down?

10. and more...?

There is much to be explored in these regions of transition that will enrich our understanding of both nuclear and quark physics.

III. THE EXPERIMENT

A. Experiment Design

1. Overall Plan

We divide the experiment into five sections with design requirements and running conditions slightly different for each.

1. Elastic e-d with e and d detected in coincidence.
2. Low Q^2 threshold inelastic e-d*.
3. Low Q^2 quasi elastic scattering.
4. High Q^2 threshold inelastic e-d*.
5. Single and double arm elastic scattering from hydrogen for calibration.

The scattered electrons will be measured in the 1.6 GeV spectrometer, and for elastic scattering, the recoil nuclei will be detected in the 8 GeV spectrometer. A plan view of the experimental layout is shown in Fig. III.1. Schematics of the kinematic regions to be covered are given in Figs. III.2 and III.3.

To make measurements with the most sensitivity to the magnetic structure functions and to minimize the final errors it is critical to make the backward angle measurements at as large an angle as possible. The overall design is most affected by the following factors:

1. The kinematics for elastic and threshold inelastic scattering. See the tables below.
2. The expected low cross sections at high Q^2.
3. The angular and energy ranges of the spectrometers:

Spectrometer	Angle
1.6 GeV	$37° \leq \theta \leq 155°$
8.0 GeV	$12° \leq \theta$

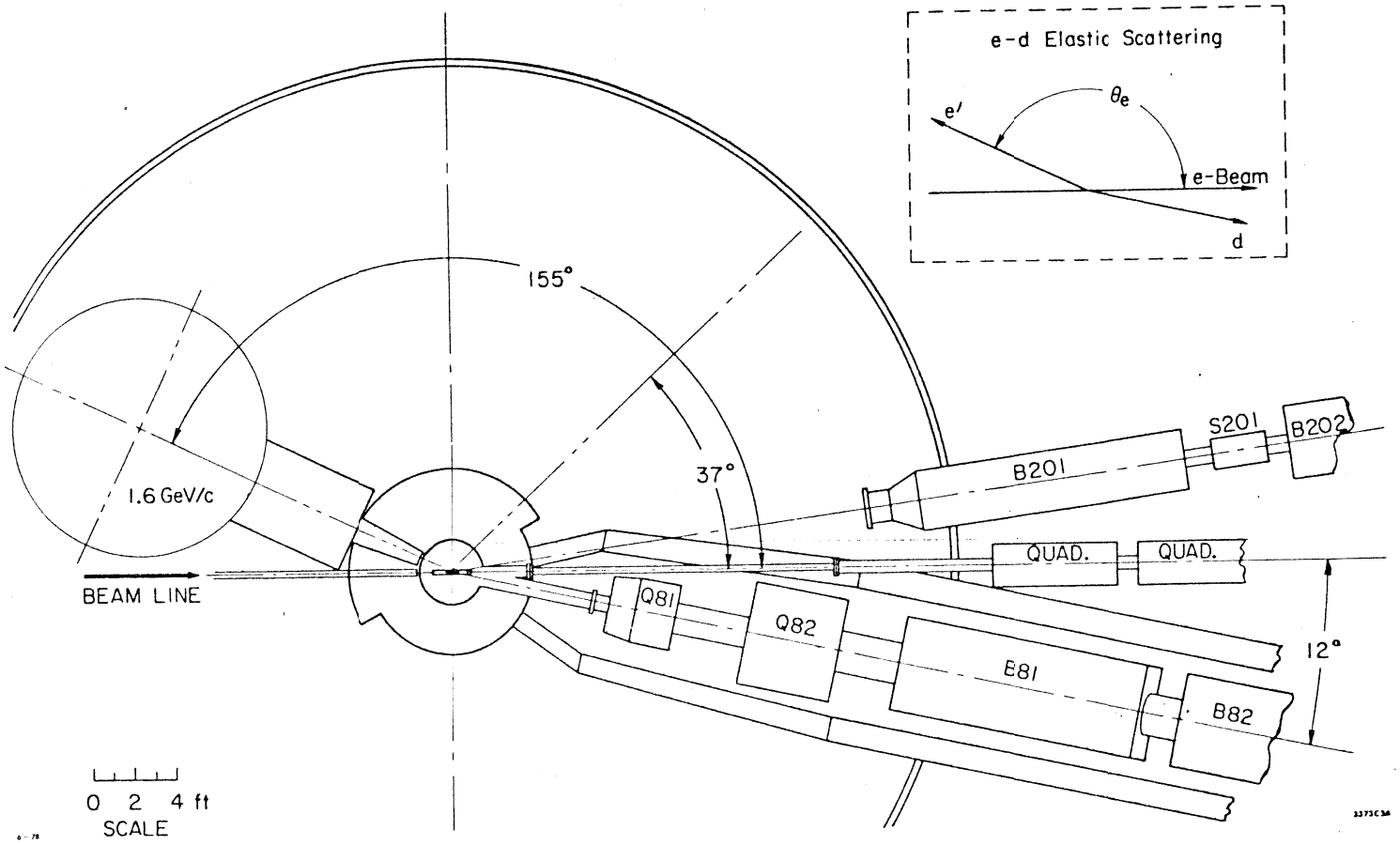

Fig. III.1. Plan view of the proposed experimental layout. Indicated are the target and pivot area with the 1.6 GeV spectrometer set at 155° and the 8 GeV with the movable scattering chamber connected set at 12°, the downstream beam pipe, and two quadrupoles to focus the transmitted beam into the beam dump. The 20 GeV spectrometer will be parked out of the way at about 7°.

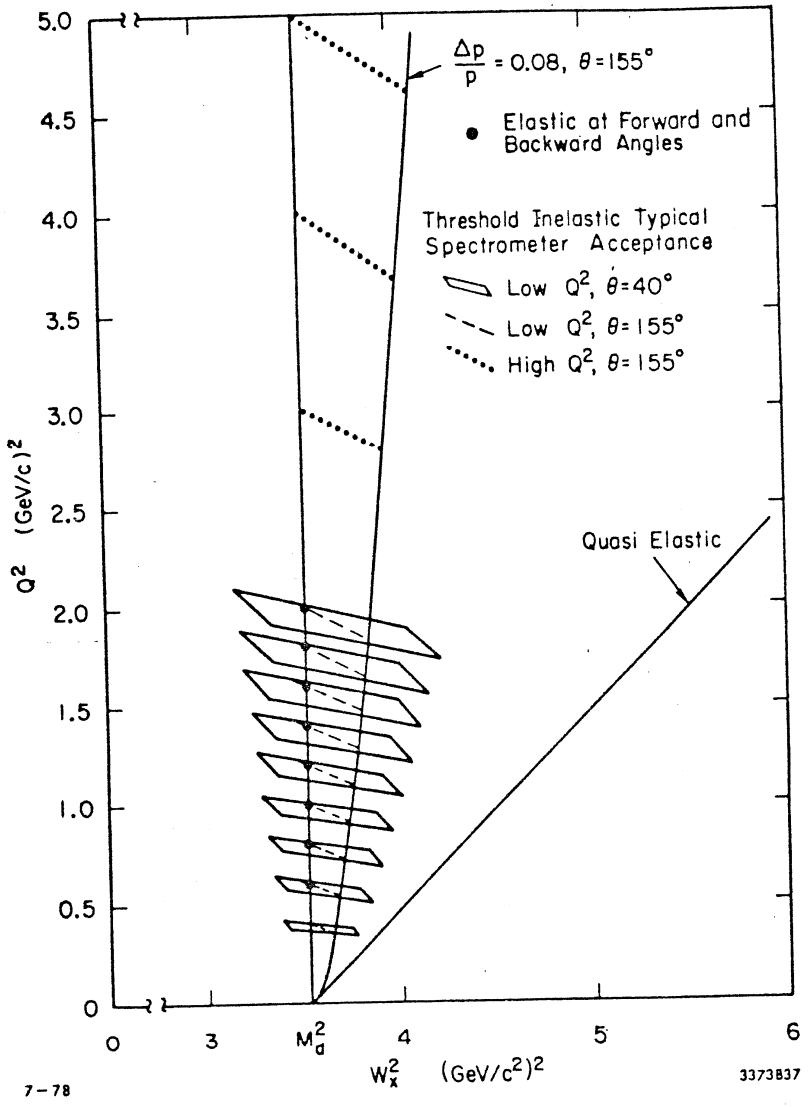

Fig. III.2. Kinematic regions for elastic scattering and low and high Q^2 threshold inelastic scattering.

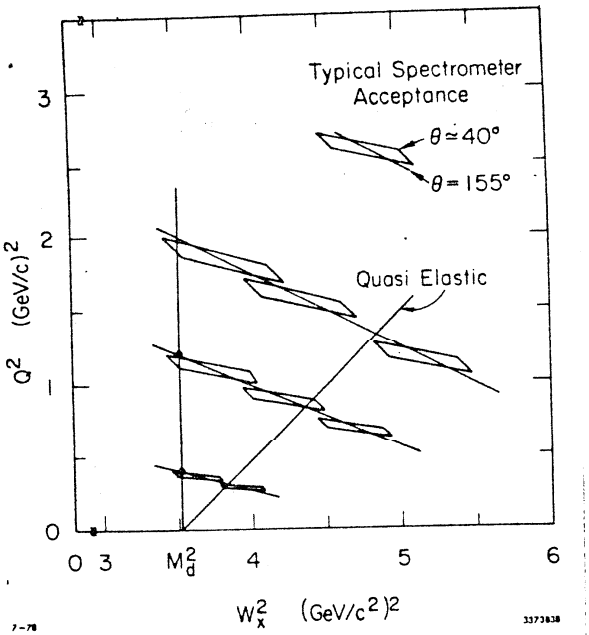

Fig. III.3. Kinematic regions for quasielastic scattering.

These angular ranges take into consideration that the 20 GeV spectrometer must be fixed at about 7° and a four-inch beam pipe will be used just after the scattering chamber for the transmitted beam.

4. Multiple Coulomb and nuclear scattering of the recoil deuterons in the target and window materials.

5. Energy loss by ionization for the incident electrons at the rate of 0.342 MeV/cm in LD2 and deflection by multiple Coulomb scattering.

With these conditions in mind we designed the experiment with ingredients as follows:

ii) Beam

To provide an electron beam with energy 0.4 to 2.9 GeV with intensity up to 100 mA peak current we propose that Injector East be built

(See Appendix A). We expect that this injector will provide maximum beam currents roughly as indicated in Fig. A.2 with beam quality comparable to the present high energy SLAC beams at high intensity, i.e., 80% transmission through $\pm$ 0.2% slits (B6).

iii) Target and Scattering Chamber

The target design is influenced mostly by factors 2., 4., and 5. above. The one we propose is a variation on the now familiar SLAC (J. Mark) LH_2 and LD_2 targets. It would consist of five cells, two filled with deuterium and, for calibration, two filled with hydrogen, plus one empty cell. The cells would be cylinders 20 and 40 cm long and approximately 3 cm diameter made of thin mylar mounted in cantalever fashion from one end with liquid circulated through input and output ports connected to the usual LH_2 heat exchanger. We have studied various target designs in some detail using Monte Carlo simulations. The small diameter and thin low Z walls in the proposed design are chosen to minimize scattering and absorption of recoil nuclei. Two lengths are chosen to cover the dynamic range of the experiment. The 40 cm targets saturate the 17 cm projected target length visible in the 1.6 GeV at 155° and would be used for the high energy parts of the experiment where counting rate is a premium and scattering and energy loss of the incident beam do not cause problems. The 20 cm targets would be used at the lower Q^2 points where counting rates will be relatively high and longer targets cause difficulties with scattering and energy loss of the lower energy beam. While the final design of the target cells is still under consideration, the proposed system is a straightforward extension of previous SLAC targets and should not present any difficulties in construction or operation.

The scattering chamber will be similar to that used for e-He scattering (SLAC experiment E121) (A4) with the 8 GeV connected directly to a moveable chamber with a sliding vacuum seal top and bottom and a thin hymen between the 8 GeV and chamber vacuum systems. We anticipate using pieces of the previous chamber by reworking it to provide entrance and exit ports in a configuration consistent with the angular requirements of this experiment.

iv) Spectrometers

The 8 GeV will be equipped with the very simple scintillator trigger counters plus dE/dx counters used in E121. There will be no p - θ hodoscopes in the 8 GeV.

For the scattered electrons we would require three basic detectors:

1. A simple set of two or three planes of scintillator trigger counters.
2. A shower counter for electron identification.
3. A set of proportional wire chambers for track reconstruction.

Since we are looking at scattered electrons very near the elastic peak and often below pion threshold, the π/e ratio will always be small. Therefore, to distinguish electrons we need only a shower counter and no Cerenkov counter. There already exists a lead glass shower counter for the 1.6 GeV (B6) that we anticipate using, if it is available.

The major detector development for this (and possible future) experiment(s) is a set of four planes of wire chambers for the 1.6 GeV. These are critical for the success of this experiment, and they are essential for

obtaining high quality data. Used in conjunction with the trigger counters and the shower counter, they perform two major functions:

1. They are used to separate single electron events from possible multiple particle events and other junk.
2. By using the measured single particle tracks and the 1.6 GeV optics coefficients (B6) we will reconstruct the momentum, angle, and projected x_o position in the target for the scattered electrons.

In the single arm measurements we are aiming for good overall resolution in E_f (2 to 3 MeV) to be able to study the details of the inelastic threshold region. With very thin targets, such resolution could readily be achieved with the incident beam and the 1.6 GeV spectrometer with wire chamber hodoscopes. For thick targets the dE/dx loss for the incident electrons causes the incident beam to be shifted down and slightly straggled in energy as it passes through the target. Using a 40 cm target at 155° at $Q^2 = 0.6\ (2.0)\ (GeV/c)^2$ this corresponds to a 4.0% (2.7%) shift in the apparent incident energy. Therefore, without any correction, the overall resolution would be dominated by the spread due to ionization losses of the incident electrons and would be intolerable for our single arm experiments.

However, by measuring the electron tracks using wire chambers in the 1.6 GeV, the x_o position of the event can be reconstructed to something better than $\pm$ 2 cm, which corresponds to a dE of $\pm$ 1.6 MeV when projected onto the target length viewed at 155°. A correction can be made to the measured electron momentum which improves final resolution by better than a factor of four over what is apparent with no correction. With this correction we would expect to achieve resolutions in E_f at $Q^2 = 0.6\ (2.0)\ (GeV/c)^2$ of

Table I

RESOLUTION FOR e-d SINGLE ARM

Q^2 $(GeV/c)^2$	θ (Degrees)	E_i (GeV)	(1) $\pm\Delta E_i$ (MeV)	(2) $\pm\Delta E_i$ (MeV)	(3) $\pm\Delta E_f$ (MeV)
0.6	27	1.741	3.48	1.50	3.44
	155	0.485	0.97	1.62	1.24
1.0	34	1.848	3.69	1.22	3.33
	155	0.622	1.32	1.62	1.25
2.0	44	2.133	4.27	0.984	3.32
	155	1.038	2.08	1.62	1.28
5.0	155	1.991	3.98	1.62	1.42

(1) Spread in incident energy from ± 0.2% slits

(2) Spread in incident energy from dE/dx in ± 2 cm x_o projected.

(3) Spread in scattered energy = $[(1) + (2)]^{\frac{1}{2}}$/Recoil.

approximately ± 1% (± 0.6%) and still take full advantage of long targets.

In Table I we show a few values for the expected overall resolution in the scattered electron energy E_f. We have assumed the energy defining slits are at ± 0.2% and that the projected X_o resolution is conservatively ± 2 cm. From this table it is apparent that we will not clearly resolve the elastic peak in the deuteron with this system (BE = 2.2 MeV). For most kinematic points the resolution would be dominated by the spread in incident beam energy with the slits open at ± 0.2%. For the elastic scattering, where counting rate is precious and electron energy resolution is not important in the coincidence experiment, we would run with wide slits (± 0.5% or so). For the threshold inelastic running, where counting rates are relatively high and single arm resolution is important, we would run with slits closed to 0.1 to 0.2%, and depend on the x_o reconstruction to achieve resolution of ± 1.5 to 3 MeV in E_f.

The design and construction of the wire chambers would be patterned after successful systems already used at SLAC and other places. They would contain two sets each of two orthogonal planes, one located near the exit of the spectrometer and one located near the p focus. The approximate size would be 40 × 60 cm with 1000 wires at 2mm spacing. A CAMAC readout of 7 LRS 2720 units, or the equivalent, would be required. We expect that the chambers would be built at SLAC to our specifications and maintained by the spectrometer Facilities Group for general use.

v) Beam Dump

Because of the long targets and relatively low energy (for SLAC) electron beams, the beam dump requires some special considerations. The

electron multiple scattering in the targets disperses the transmitted beam so that it would not arrive at Beam Dump East (BDE) 144 m from the target without assistance. The plan is to use two quadrupoles in the exit beam line positioned at about 10 m downstream from the target. These should be 10-inch I.D. quads such as the 10Q36 spare quads available on loan from Argonne National Laboratory. They will be placed as close to the target as is consistent with setting the 8 GeV spectrometer at 12°. The beam pipe would be four inches in diameter near the scattering chamber so as to give clearance at Q81 when the 8 GeV is at 12°. A 10-inch diameter pipe would be used inside the quadrupoles and beyond to the entrance to the dump. We calculate that this configuration would transmit 99% (>>99%) of a 0.4 (2.0) GeV/c beam to the dump. Some shielding may be necessary around the beam pipe to reduce the low energy background in the 8 GeV spectrometer.

vi) Electronics and Computer

The high speed electronics requirements for this experiment to be provided by the SLAC High Energy Electronics Pool will be similar to those for E101 and E121. Rough estimates are:

Type of Unit	Channels
Discriminator	40
Coincidence	20
ADC	12
TDC	12

There will be additional requirements for the proposed PWC's for the 1.6 GeV which are not specified at this time.

The ESA computer will be required for checkout and online data taking and some preliminary analysis, tape copying, and sifting for the customary period before and after the experiment.

vii) Analysis

We anticipate the analysis will follow a three-step process patterned after that used for E101, E121, and E133. After some initial data sorting and condensing on the ESA computer, the bulk of the analysis will be done on the SLAC Triplex. In conjunction with the data analysis, there will be some Monte Carlo modeling of absorption and scattering of recoil nuclei and spectrometer acceptances. Much of the programming for all three steps exists or could be readily adapted from our previous work. We estimate the SLAC Triplex resource requirements to approximately as given in Table II.

Table II.

ESTIMATED SLAC TRIPLEX RESOURCE REQUIREMENTS

Catalogued data tapes	30 to 50
Mountable private disk packs for program backup and large temporary data sets	1
Computer units for WYLBUR editing and CPU time	2,000,000

viii) Errors

In a Rosenbluth separation of $B(Q^2)$ using large and small angle (θ_L, θ_S) measurements

$$B = \left[\frac{\sigma(\theta_L)}{\sigma_{mott}(\theta_L)} - \frac{\sigma(\theta_S)}{\sigma_{mott}(\theta_S)} \right] / [\tan^2(\theta_L/2) - \tan^2(\theta_S/2)] \qquad \text{III.1}$$

If $\tan^2(\theta_S/2) << \tan^2(\theta_L/2)$ and the statistical error associated with the small angle (high counting rate) measurement can be neglected, the statistical error for the separation is

$$\frac{\delta B}{B} \sim C \sqrt{\frac{A}{B}} \frac{\cos^2(\theta_L/2)}{B} + \frac{\sin^2(\theta_L/2)}{A} \qquad \text{III.2}$$

where C is a slowly varying function of incident energy and angle. In our experiment, where B/A is expected to be a few percent, $B \tan^2(\theta_L/2)/A << 1$ and this simplifies to

$$\frac{\delta B}{B} \sim C \frac{\sqrt{A}}{B} \cos(\theta_L/2) \sim \frac{C\sqrt{A}}{2B} (\pi - \theta_L) \qquad \text{III.3}$$

Thus, to minimize the error, we will do the experiment at the largest θ_L consistent with the limitations of the 1.6 and 8 GeV spectrometers. The running conditions for elastic scattering are shown in Table III where an asterisk (*) indicates the kinematic quantity at the limit of its range that determines the settings for each point.

The systematic error in B depends on the absolute values of the spectrometer acceptance, beam current accidental rates, dead time, radiative corrections, π rejection, etc. Since B is derived from the small difference

between measured quantities, it is critical that the error in the relative normalization between the data at the two angular settings be kept small. For this reason the same spectrometers are used for forward and backward measurements, the target is long enough to saturate the acceptance at both angles, and enough time is given for small angle measurements (low beam current) to keep the dead time and accidental corrections small and the wire chamber efficiencies rate independent. These effects are expected to add up to less than 3 to 5% relative systematic error. Such a relative normalization error between the small and large angle measurements $\delta N/N$ affects the measurement of B by

$$\frac{\delta B}{B} \sim \frac{A}{B \tan^2 (\theta_L/2)} \frac{\delta N}{N} \qquad \text{III.4}$$

The consequences of a 3% relative systematic error are shown in Table III, assuming A and B from Gari and Hyuga using Reid soft-core plus MEC (D2). A similar systematic error will affect the single arm measurements.

An important part of the proposed experiment will be to take data using a proton target. We will measure single and double arm elastic scattering at forward and backward angles from short and long targets, with different counting rates, and with the elastic peak in different parts of the spectrometer acceptance. From this data we will derive absolute proton cross sections to be compared with the world's measured values. By this comparison, and by internal consistency checks, we can check all the procedures used to deduce $B(Q^2)$ for the deuteron. We can explore the effects of counting rates, solid angle variations, etc., and get a good understanding of the corrections and knowledge of the uncertainties in the absolute normalization between the forward and backward angle measurements.

III. EXPERIMENT

B. Run Plans

Tentative run plans for four divisions of the experiment are given in Tables III, IV, V, and VI. The total number of hours of requested beam time is summarized in Table VII. The values of Q^2 and the counting rates and division of hours shown there are, for example, only to illustrate how the requested time might be apportioned given certain assumptions about the cross sections. The final run plans will be adjusted to meet the actual circumstances. In particular, at the lower Q^2 points from 0.4 to about 1.0 $(GeV/c)^2$ where the rates are high, the short counting times are determined mostly by the setup time and by the maximum allowed singles rates. At higher Q^2 the number of data points and the running time will be determined by the size of the cross sections, which at this time is a secret known only to Mother Nature.

It would be possible to schedule the beam time with Injector East running at 180 pps in the last five sectors of the linac using modest amounts of electric power simultaneous with delivering other full energy beams in the other 180 pulses. An alternative plan, which we would favor for the low counting rate portions of the experiment, would be to schedule part of the requested hours to occur in a period (perhaps one calendar month) during a machine shutdown at the end of a normal run cycle. During this time Injector East and five sectors of the linac could run at 360 pps, and the beam switchyard, and ESA could continue to operate at considerably reduced power levels as compared to full linac operations. Running at 360 pps would speed up the real data taking time and might reduce the impact of this experiment on the demands for ESA resources.

We note, also, that the Director of the Stanford Synchrotron Radiation Laboratory (A. Bienenstock, private communication and letter attached) has expressed interest in using the new injector to fill the SPEAR storage ring with electrons when they are using the ring for synchrotron radiation research. Thus, our running time might nicely coincide with one of the upcoming periods of dedicated SSRL running at SPEAR after PEP is turned on with considerably reduced costs for injecting electrons into the ring.

Table III

RUN PLAN FOR e-d ELASTIC SCATTERING

Q^2 (GeV)	θe (Degrees)	E_i (GeV)	E_f (GeV)	P_r (GeV)	θ_r (Degrees)	Counts/Hr. (RSC + MEC)	Hours 100% Eff.	ΔB/B Stat. (%)	ΔB/B Syst. (%)
0.6	37*	1.3032	1.1432	0.7909	60.45	44,000	2	7.7	1.6
	150	0.4888	0.3289	"	12.00*	1,584	2		
0.8	37*	1.5201	1.3068	0.9195	58.80	14,050	2	8.0	2.2
	148	0.5839	0.3707	"	12.34*	360	2		
1.0	37*	1.7147	1.4481	1.0349	57.36	5,463	2	13.	3.9
	147	0.6715	0.4050	"	12.31*	110	4		
1.2	37*	1.8935	1.5737	1.1412	56.09	2,468	2	21.	6.5
	146	0.7546	0.4347	"	12.30*	42	10		
1.4	39	1.9687	1.5955*	1.2407	54.03	941	3	26.	8.2
	145	0.8343	0.4612	"	12.31*	17	25		
1.6	41	2.0317	1.6053*	1.3349	52.09	408	3	34.	11.
	144	0.9116	0.4851	"	12.33*	7.8	55		
1.8	43	2.0859	1.6061*	1.4248	50.24	182	3	53.	15.
	143	0.9868	0.5071	"	12.37*	3.9	80		
2.0	45	2.1334	1.6004*	1.5113	48.48	90	5	80	25.
	142	1.0604	0.5274	"	12.41*	2.0	80		

Total Hours - 280

*Quantity is at the limit of its range and determines the settings for that data point.

(For other information regarding the table, see the following page.)

Table III (Cont.)

Assumptions

Beam: Current as a function of incident energy from Injector East, Fig. A2, with 1.6 μs pulse width at 180 pps, slits ± 0.5%.

Target: 40 cm.

Spectrometers: 1.6 - 8 GeV combination, Solid angle from Monte Carlo.

Cross Section: Reid soft-core plus MEC by Gari and Hyuga, Ref. (D3), (see Fig. II.8).

The last two columns show the statistical errors and the systematic errors assuming a 3% uncertainty in the relative normalization of the forward and backward angle measurements.

Table IV

RUN PLAN FOR LOW Q^2 THRESHOLD INELASTIC SCATTERING

$\theta = 155°$

Q^2	$\frac{d\sigma}{d\Omega dE}$ $(cm^2/sr/MeV) \times 10^{-37}$	Counts/Hr. in 3 MeV Bin at Threshold	Hours
0.4	4.0	1580	2
0.6	3.0	1180	2
0.8	2.0	792	2
1.0	1.0	390	2
1.2	0.7	280	4
1.4	0.4	160	6
1.6	0.3	120	8
1.8	0.2	80	10
2.0	0.1	40	20
		Total Hours at 155°	56
		Total Hours at 40°	20

Assumptions

Beam: 50 mA, 180 pps, Slits ± 0.1% to ± 0.2 %

Target: 40 cm

Spectrometer: 1.6 GeV at 40° and 155°

Cross Section: Nonrelativistic impulse approximation from Fabian and Arenhovel (G7, G8), (Fig. II.15.)

Table V

RUN PLAN FOR QUASI ELASTIC SCATTERING

Q^2 At ed Elastic $(GeV/c)^2$	θ (Degrees)	Spectrometer Bites (Approximately)	Hours
0.4	40	6	5
	155	6	5
1.2	40	10	10
	155	10	10
2.0	40	12	30
	155	12	40
		Total Hours	100

Assumptions

Beam: 50 mA, 180 pps, Slits ± 0.2%

Target: 40 cm

Spectrometer: 1.6 GeV at 40° and 155°

Cross Section: e p quasi elastic, dipole form factors. With data binned in 5 MeV bins in E_f, the counting time is determined to achieve 5% statistics in the bin with the lowest counting rate in a given spectrometer bite.

Table VI

RUN PLAN FOR HIGH Q^2 THRESHOLD INELASTIC SCATTERING

Q^2 $(GeV/c)^2$	E_i (GeV)	E_f (GeV)	$\frac{d\sigma}{d\Omega dE}$ $(cm^2/sr \cdot MeV)$	Counts/ Hour	Hours
3	1.372	0.565	2.1 (-40)	2.4	16
4	1.687	0.612	1.8 (-41)	0.2	34
5	1.991	0.648	4.4 (-42)	0.05	100
				Total Hours	150

Assumptions

Beam: 100 mA, 180 pps, Slits ± 0.2%.

Target: 40 cm

Spectrometer: 1.6 GeV at 155°.

Cross Section: R → small at threshold (see Fig. II.26).

Table VII

REQUESTED NUMBER OF HOURS OF FIVE-SECTOR BEAM USING INJECTOR EAST AT 180 pps.

	Experiment	Hours
1.	Elastic e-d coincidence	280
2.	Low Q^2 threshold inelastic e-d* single arm	75
	Background at low Q^2	25
3.	Quasi elastic single arm	100
	Background for quasi elastic	25
4.	High Q^2 threshold inelastic e-d* single arm	150
	Background at high Q^2	30
5.	Hydrogen calibration	40
	Total hours at 100% efficiency	725
	25% inefficiency	245
	Total hours at 75% efficiency	970

IV. POSSIBLE FUTURE PROJECTS

A. Experimental Facilities Development

The availability of high intensity electron beams in the energy range 0.4 to 2.9 GeV from the proposed new injector would open up the possibility for other experiments in nuclear systems besides the one we are proposing here. There are, however, two major disadvantages to the new beam for nuclear physics experiments: a) at the low duty factor (5×10^{-4}), and b) the limited resolution. The raw beam will have resolution of roughly $\pm$ 0.2%, and the A-bend slits can be narrowed to $\pm$ 0.1% with a corresponding loss in analyzed beam current. Therefore, the beam as proposed would be most useful for medium resolution single arm inelastic inclusive experiments where high intensity is required but the nuclear final states are generally not resolved, and for elastic coincidence experiments which pick out highly correlated final states. The low duty factor is not likely to be improved significantly in this energy range until a new accelerator (K5) is built (if ever).

We do know of one way, with a modest investment, to dramatically improve the energy resolution of the Injector East beam which would greatly enhance its usefulness for higher resolution experiments at high intensity in the 1 to 3 GeV region. To do that we would follow the suggestion (K6) of R. Miller and G. Loew (SLAC) and build an energy compression system in the beam switchyard. This device, called the Monochromat (described in detail in Appendix B), uses a section of accelerator cavities, designed for a radio-frequency particle separator, to compress the energy spectrum of the dispersed beam in the middle of the A-bend, at some sacrifice in increased angular emittance. Miller and Loew estimate that such a system could produce electron beams with a momentum

spread $\Delta p/p$ of approximately 0.01% with little or no loss in intensity. The increase in angular emittance would be well within the range acceptable to most scattering experiments. While such beam resolution would slightly exceed the limiting resolutions of the spectrometers in ESA, it could be put to many uses, especially in scattering experiments in the light nuclei.

B. Future Experiments

i) Physics Motivation

Our present interests are centered around the few nucleon systems where with clean electromagnetic probes at large momentum transfer we hope to learn important features of the interaction of nucleons at short distances. Given the investment in Injector East for this experiment and possibly in the Monochromat in the future, we could significantly increase the physics return on that investment by making elastic and inelastic scattering measurements on ^{3}He and ^{3}H similar to the ones proposed here for deuterium. The physics questions to be probed are similar to those for the deuteron except that with three nucleons in different isotopic combinations we have the opportunity to extend the explorations to such questions as:

1. How far can we go toward understanding the structure of the three-nucleon system by using the fundamental two-nucleon interaction as we know it from NN scattering and the deuteron as input to a many-body formalism, such as the Faddeev or variational schemes? Can we use the structure functions of these two nuclei to tell us in the clear way about aspects of the NN interaction not available from the two-nucleon system, such as possible three-body forces?

2. Can we learn something from the magnetic structure functions F_{mag} that might lead us to understand why the Faddeev calculations for the charge form factor of ^3He do not get good agreement with the data in the position of the diffraction minimum and the height of the second maximum? This is a problem which has plagued the three-body calculations now for several years.

3. What role do relativistic wave functions, meson exchange, and isobar currents play in the three-body nuclei? Is it possible to learn things about these features by comparing the data from two isotopes where the effects may be different?

4. If MEC effects are large in the magnetic structure functions, as has been suggested (I9), can we confirm some of the details of those currents that we might learn from the I = 0 deuteron by comparing with the results from these $I = \pm 1/2$ systems: e.g., What diagrams are important?; What are the strengths and momentum dependences of the vertex functions?; etc.

5. And more...

There are many investigations of the three-nucleon systems addressing some of these problems (I1-I12). We will give one example here which illustrates the power of the knowledge of magnetic structure functions at large Q^2 for resolving some of these questions. Figs. IV.1 and IV.2 show the results of a claculation by Barroso and Hadjimichael (I9) of F_{mag} for ^3He and ^3H respectively. They give results for the contributions from the

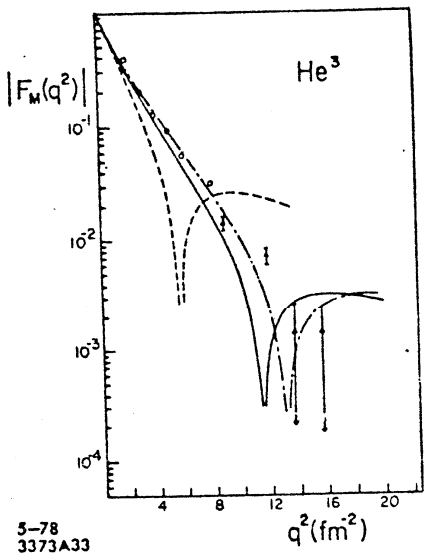

Fig. IV.1. The magnetic form factor of ^{3}He, from Barroso and Hadjimichael (I9). The curves are: solid: (S-S) + (D+D) state impulse contributions; dashed: (S-S) + (D-D) + (S-D) impulse contributions; dot-dashed: total impulse plus MEC terms. The data is from Refs. (C1) and (C2).

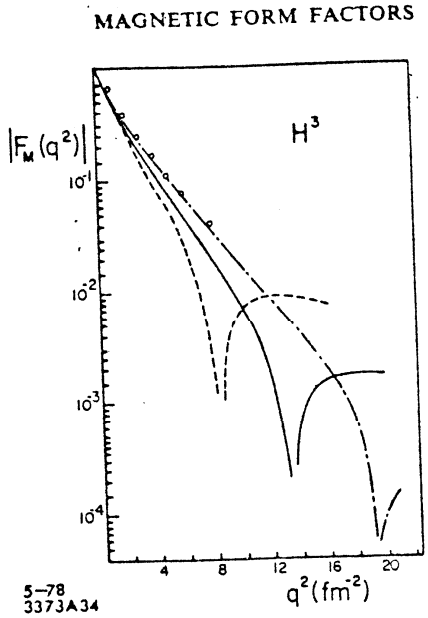

Fig. IV.2. The magnetic form factor of ^{3}H, from Barroso and Hadjimichael (I9). The curves are as in Fig. IV.1, and the data are from Ref. (C3).

impulse approximation from S state and D state matrix elements, and a curve which includes the interference terms from S-D matrix elements. They have also calculated the MEC contributions. As these curves show, there are large effects on the diffraction features in F_{mag} in both nuclei from the inclusion of the S-D interference terms and from the MEC terms. This is similar to the situation described in Section II.B for deuteron electrodisintegration at threshold. The shifts are in opposite directions. In ^{3}He they nearly compensate exactly, while in ^{3}H the total structure function is considerably shifted from that with no S-D interference terms or MEC contributions. The presently available data for F_{mag}, also shown in

these figures, is inadequate to probe the interesting regions around the diffraction minima.

The best comparison with theory can be made when F_{ch} and F_{mag} are separately known. For a spin 1/2 nucleus, the structure function $A(Q^2)$ is given by

$$A(Q^2) = F_{ch}^2 + \tau(1+K)^2 F_{mag}^2/(1+\tau) \qquad \text{IV.1}$$

where $\tau = Q^2/4M^2$ and K is the nuclear anomalous magnetic moment. $B(Q^2)$ is a function of F_{mag} only. At large Q^2, $A(Q^2)$ can have substantial contributions from the magnetic structure function F_{mag}, depending on the relative size of F_{ch} and F_{mag}. In ^{3}He (^{3}H) the anomalous moment K is -4.2 (7.94), and therefore, at $Q^2 = 2$ (GeV/c)^2 for example, the factor $\tau(1+K)^2$ is 0.6 (5.1). In our previous forward angle experiment (A5) we have measured $A(Q^2)$ for ^{3}He out to $Q^2 = 3$ (GeV/c)^2 (see Fig. IV.3). A spearation of F_{ch} and F_{mag} for ^{3}He at large Q^2 would complement that measurement and make possible a much more useful comparison with theory.

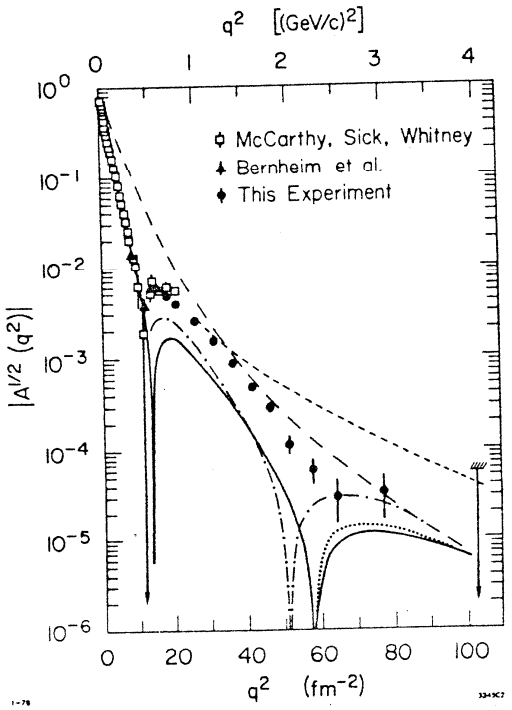

Fig. IV.3. ^{3}He elastic structure function $A(Q^2)$ at large Q^2. The data are from Refs. (A5), (C1), (C2). The curves are: solid, Faddeev NRIA (I5); dot-dashed, NRIA plus MEC (I13); small-dashed, a preasymptotic version of the dimensional scaling quark model (J3); large-dashed, relativistic impulse approximation for asymptotic Q^2 (J4, J5).

ii) The Experiments

The experiments we have in mind are elastic and inelastic scattering at forward and backward angles to separate the F_{ch} and F_{mag} and the νW_2 and $2MW_1$ in Rosenbluth plots. In parallel with the present proposal, we have made detailed Monte Carlo studies of target designs, and have investigated the suitability of the proposed new injector beam and the spectrometer setup for exploring the kinematic range for elastic and threshold inelastic scattering at large Q^2. This study indicates that suitable targets can be built, and that the projected counting rates are high enough to yield good measurements for F_{mag} way beyond the range of previous experiments.

For the ^3He targets long cylindrical cells made of thin mylar would be used containing high pressure gaseous helium circulated to a LH_2 heat exchanger. Such a system could use much of the high pressure ^3He gas system developed for E121. Target cells of 1 to 3 cm diameter with mylar walls 0.003 to 0.010 inch thickness containing gas at 20° K at 5 to 50 atm could be used to cover most of the dynamic range of the experiments, giving adequate counting rates with tolerable losses of recoil nuclei due to absorption and scattering in the target and window materials.

For ^3H we have considered several designs. (This preliminary study of ^3H targets cells has been done in collaboration with J.S. McCarthy of the University of Virginia, Charlottesville, Virginia.) The simplest and safest system would be cylinders of Fe or Al filled with ^3H at the source away from the SLAC site and permanently sealed at high pressure (10 to 200 atm) at room temperature. These would then be heat sinked to liquid nitrogen in an isolated scattering chamber with various levels of safety mechanisms for trapping and absorbing the ^3H if it were to be released from the cells. For

example, a volume of activated Fe-Ti powder would be available in the scattering chamber to act as a getter for ^3H by forming metal hydrides. A ^3H target of similar design was used in the electron beam at Stanford in 1965 (C3),

The higher resolution from the proposed monochromat would be of particular advantage in these experiments. We can see this by looking at some typical values of parameters governing the single arm resolution. Since the density of gas in the targets is relatively low as compared to LD2, the dE/dx spread of the incident beam energy in the long targets is proportionally smaller. Some typical values for dE/dx in ^3He and ^3H targets are given in Table VIII. In Table IX we show some typical values of the beam energy spread in MeV for the range of kinematics for Rosenbluth separation in these nuclei. We assume two possible beams: a) no monochromat with resolution at $\pm$ 0.2% determined by the A-bend slits, and b) using the monochromat with resolution conservatively estimated at $\pm$ 0.02%. To perform single arm elastic scattering we require the total resolution to be at or below $\pm$ 2 MeV to resolve the elastic peaks from two-body breakup threshold about 5 MeV away. The total resolution in the final electron energy for a given target would roughly be the rms sum of the right hand column in Table VIII with the entries in Table IX.

It is apparent from Tables VIII and IX that, assuming a projected x_0 resolution of $\pm$ 2 cm, the overall resolution is dominated by the incident beam spread, and that single arm experiments would be marginal or impossible over much of the required range using only the A-bend slits.

However, if the monochromat beam were available, we could easily resolve the elastic peaks in single arm measurements over the entire range of Q^2. The availability of the high resolution beam could extend the

Table VIII

TYPICAL VALUES FOR dE/dx IN ^{3}He AND ^{3}H TARGETS

	dE/dx (MeV/cm)	dE in 40 cm (MeV)	$\pm\Delta E_f$ (MeV)
^{3}He at 20° K			
10 atm	0.0667	2.66	0.2
50 atm	0.295	11.8	0.9
^{3}H at room temperature			
30 atm	0.018	0.72	0.06
100 atm	0.061	2.44	0.19

Typical values for energy loss dE/dx by the incident electron beam in ^{3}He and ^{3}H targets and the resulting contribution to the spread in the scattered electron energy for $Q^2 = 2$ (GeV/c)^2 at 155° with projected x_0 resolution of ± 2 cm.

Table IX

KINEMATIC SETTINGS FOR e-^{3}He AND e-^{3}H

ELASTIC SCATTERING AND TYPICAL VALUES FOR BEAM ENERGY SPREAD

Q^2 ((GeV/c)^2)	θ (Degrees)	E_i (GeV/c)	$\pm\Delta E_f$ $\pm$ 0.2% Slits (MeV)	$\pm\Delta E_f$ $\pm$ 0.02% Monochromat (MeV)
0.8	30	1.655	5.7	0.57
	155	0.454	1.4	0.14
2.0	50	1.926	6.2	0.62
	155	0.924	2.3	0.23

The contribution to the spread in scattered electron energy E_f from the spread in the incident beam for the range of kinematic settings for e-^{3}He and e-^{3}H elastic scattering.

sensitivity of such measurements by factors of five or ten for two reasons: a) since the recoil nuclei are not detected, the target walls can be made much thicker and the gas density increased, limited only by safety and the strength of materials and by the dE/dx effect on the electron resolution; b) the electrons can all be detected at the maximum angle of the 1.6 GeV spectrometer, $\theta = 155°$, because the 12° minimum angle of the 8 GeV is not a limiting factor, and most important, we can ignore the fate of the recoil nuclei in the thick walls. The sensitivity of the final errors is a strong function of the electron angle because of the large lever arm in $\tan^2(\theta/2)$ for angles above 130°.

The monochromat beam would be particularly important for the ^3H measurements. A 30 atm room-temperature target, for example, would require approximately 0.010-inch thick Al walls, which would make the target unsuitable for any coincidence experiments below Q^2 approximately 0.8 $(GeV/c)^2$, while for higher Q^2 the electron angle would be limited to about 130°. At larger angles the recoil nuclei go farther forward and pass through too much Al. A 100 atm target would require approximately 0.032-inch thick Al or 0.010-inch Fe walls and could not be used at all for coincidence experiments. However, with the monochromat beam, a 100 or 200 atm target could be used in single arm, thus greatly extending the sensitivity of the ^3H measurements. By using Fe instead of Al target cells the safety factor would also be much improved.

The [illegible]ments would, of course, have to contend with a background subtraction. For this reason also, the high resolution from the monochromat would be of enormous advantage to increase the signal/noise ratio at the elastic peak.

iii) Possible Results

To give an idea of the potential physics yield from such experiments, we display in Figs. IV.4, IV.5, and IV.6 the possible results of Rosenbluth separations of F_{ch} and F_{mag} for ^3He and ^3H. From this study we can conclude:

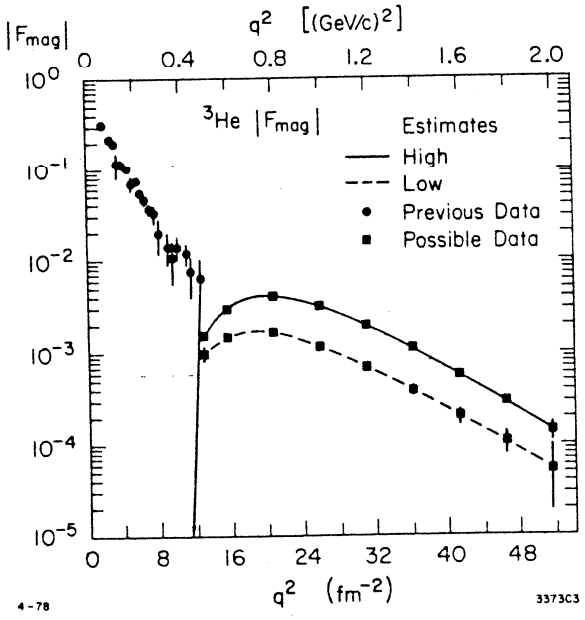

Fig. IV.4. Previous and possible data for ^3He F_{mag}. The estimates for F_{mag} have about the same shape as the measured $A(Q^2)$ and cover the range in size suggested by several calculations (I9, I10). Previous data is from Ref. (C1). The assumptions for obtaining possible data are explained in the text

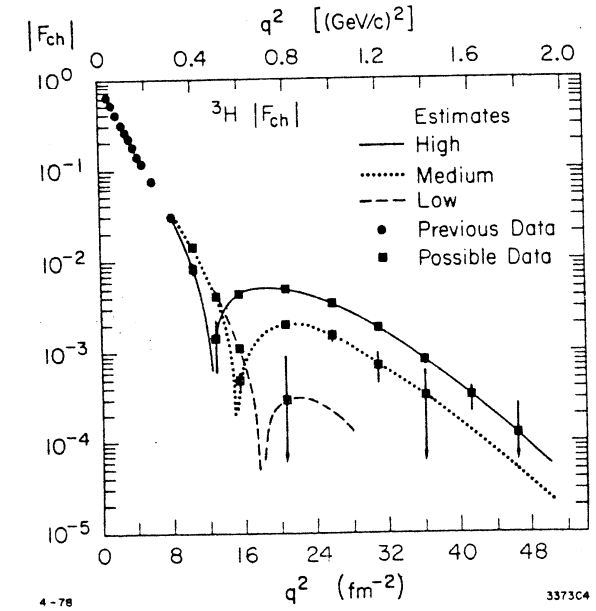

Fig. IV.5. Previous and possible data for ^3H F_{ch}. The estimates are: High, a guess similar to the measured ^3He F_{ch}; medium, similar to Faddeev calculations of Brandenburg and Sauer (I8); low, similar to Haftel and Kloet (Fig. 15 in Ref. I12) which includes contributions from NRIA plus MEC with πNN vertex form factors. The previous data is from Ref. (C3). The assumptions for obtaining possible data are explained in the text.

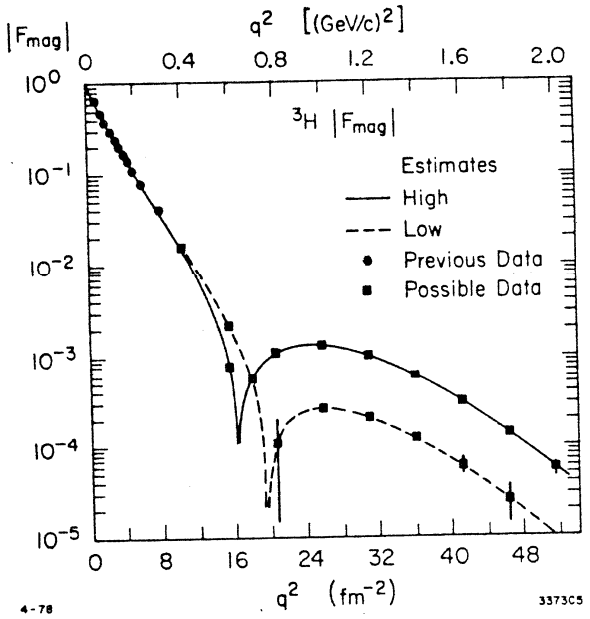

Fig. IV.6. Previous and possible data for ^3H F_{mag}. The estimates are: High, similar to the (S-S) plus (D-D) impulse contributions by Barroso and Hadjimichael (GH) (I9); Low, similar to the BH calculation including total impulse with (S-D) interference and MEC added to the above curve. The previous data are from Ref. (C3). The assumptions for obtaining possible data are explained in the text.

1. The charge and magnetic structure functions of ^3He and ^3H can be separated out to something like $Q^2 = 1.6$ $(GeV/c)^2$. This is to be compared with the possibility of measuring the sum in $A(Q^2)$ in the forward angle experiment in ^3He using high energy SLAC electron beams out to Q^2 of 3 $(GeV/c)^2$.

2. Such measurements would extend our knowledge of F_{mag}, and also F_{ch} for ^3H, by over two orders of magnitude and by factors of five or six in Q^2 over previous experiments.

3. The data would be of sufficient statistical accuracy to make a powerful probe of the diffractive features of the structure functions from which we could learn many new details of the three-nucleon system at short distance, and thus, about the basic NN interaction.

Also, if ^3H and ^3He targets are available, we would be interested in measuring the threshold inelastic and deep inelastic scattering from

these nuclei using the high energy SLAC electron beam so as to explore these two nine-quark systems with different isotopic combinations in the scaling region. From this data we would be able to study the scaling behavior of the structure functions and the ratios $(\nu W_2)^{^3H}/(\nu W_2)^{^3He}$ and $(2MW_1)^{^3H}/(2MW_1)^{^3He}$. From these ratios we might learn about the differences in quark distributions in neutrons and protons by using two nearly identical nuclear systems where the confusion due to nuclear fermi motion would nearly exactly divide out. Such measurements would compliment the existing study of σ_n/σ_p in the deep inelastic region obtained from proton and deuteron targets, the interpretation of which is plagued by uncertainties due to the Fermi motion of the nucleons in deuterium (H5-H7).

We are convinced that the physics yield from the possible future projects just described is well worth the investment in new equipment and beamtime and could yield much information about the deep structure of nuclear systems.

APPENDIX A

INJECTOR EAST

The Present Accelerator

The Stanford linear accelerator consists of a disc-loaded cylindrical copper waveguide supplied with microwave power at a frequency of 2856 megahertz. The power is provided by 245 klystron amplifiers, each capable of producing between 20 and 38 megawatts of peak power at 360 pulses per second. The output from each klystron is divided four ways to power four 10-foot sections. There are a total of about 960 sections. The accelerator is divided into 30 sectors, each 333 feet long. At the end of each sector there is a 10-foot drift section in which are located beam steering and focusing magnets and position and intensity monitors. A master trigger generator sends trigger signals at 360 pps to the pulse forming networks in the 30 sectors and to the injector station. The electron beam is bunched in the injector into a stream of bunches conforming to the 2856 MHz frequency, i.e., bunches approximately 5° or 5 picoseconds long, 0.35 nanoseconds apart. A normal full beam pulse is a train of bunches 1.6 microseconds long.

At the end of the accelerator the electron beam enters the beam switchyard which is equipped with pulsed magnets for steering the beam into different experimental areas. In Sector 11 is located a positron radiator which is used to produce a positron beam of approximately 1/20 the intensity of the electron beam that can be accelerated up to 15 GeV. The accelerator and the beam switchyard control system provide the capability for separately controlling the energy, intensity, and destination of up to eight beams for eight different experiments, each using a fraction of the maximum 360 pulses per second. The beam with which we are concerned is that in the so-called A-line. It passes through the energy dispersion magnets and the energy defining slits in A-bend

and enters End Station A (ESA). The ESA beam is directed over the pivot of three large spectrometers and then on to Beam Dump East.

The electrons gain energy at the rate of 800 MeV per sector and beam loading decreases this gain at the rate of 35 MeV/mA of peak current. To get a beam of a certain energy and intensity for energies above approximately 5 GeV, the number of sectors contributing power is adjusted until the energy is within a few hundred MeV of the desired value. Then the contribution of one sector, designated as the vernier sector, is adjusted until the desired energy is reached exactly. For beams with energy below 5 GeV, the electrons are typically accelerated in the first six sectors and then allowed to coast the rest of the way. The beam is then decelerated towards the end of the machine by backphasing the required number of klystrons. The accelerator in its present configuration is capable of delivering an electron beam in ESA ranging in energy from approximately 0.9 GeV up to 22 GeV with a maximum intensity of approximately 1 mA peak at 0.9 GeV to 50 mA peak above 10 GeV.

The maximum attainable intensity of the beam is determined by the onset of a cumulative electromagnetic instability called beam blow up or beam break up (BBU). The phenomenon is caused by the excitation of certain parasitic microwave modes in the cavities by the passage of the bunched electron beam. Some of these modes have transverse magnetic fields on the beam axis which deflect the electron bunches transversely toward the walls of the cavities where they are lost. The exact causes of the BBU phenomenon and the current threshold for the onset of the instability are a complicated function of many parameters of the beam and accelerator structures. The major factors are beam energy and current, pulse length, machine length, and the strength of external focusing applied. The BBU threshold current is approximately linear

with 1/L, where L is the accelerator length, and increases linearly by a factor of 2 with increase in energy from 2 to 20 GeV for a 30 sector machine with no focusing.

Following the discovery of the BBU phenomenon at SLAC in 1966, much effort was directed to studying its causes, verifying the scaling laws, and devising remedies to cure the problem. One of the solutions chosen was to clamp down on the radial deflection of the beam by brute force by using a system of dc and pulsed focusing quadrupoles placed all along the accelerator. With this quadrupole system, the maximum current through 1% slits into ESA ranges from 40 to 50 mA peak in the energy range from 5 GeV to 20 GeV. For beam energies below 5 GeV the intensity falls rapidly and the beam quality is not as good as at higher energy. The loss in intensity and beam quality is determined by the decrease in BBU threshold with energy, the increasingly large fractional beam loading energy loss, and by the presence of the positron radiator in Sector 11. This radiator makes it preferable to accelerate most beams to that point uniformily up to about 5 to 7 GeV. In this manner, the steering and focusing in the positron radiator area need not vary too much from beam to beam or on a pulse-to-pulse basis. However, low energy beams must then be obtained by backphasing klystrons towards the end of the accelerator as described earlier. This in turn somewhat degrades the transverse phase space. At present the lowest practical energy is around 900 MeV. During SLAC experiment E101 we managed to get a 900 MeV beam with beam currents varying from 1 to 3 mA peak through 1.7% $\Delta p/p$ slits into ESA.

The New Injector

We are proposing that a new injector, called Injector East, be constructed and installed in Sector 26 of the linac. The primary purpose of this device

is to increase the intensity and improve the quality of the SLAC electron beam at lower energies by avoiding all the problems mentioned above. This will be accomplished by removing two 10-foot accelerator sections at the beginning of Sector 26 and inserting an injector section in their place (see Fig. A.1). The electron gun will be located off the beam axis and the

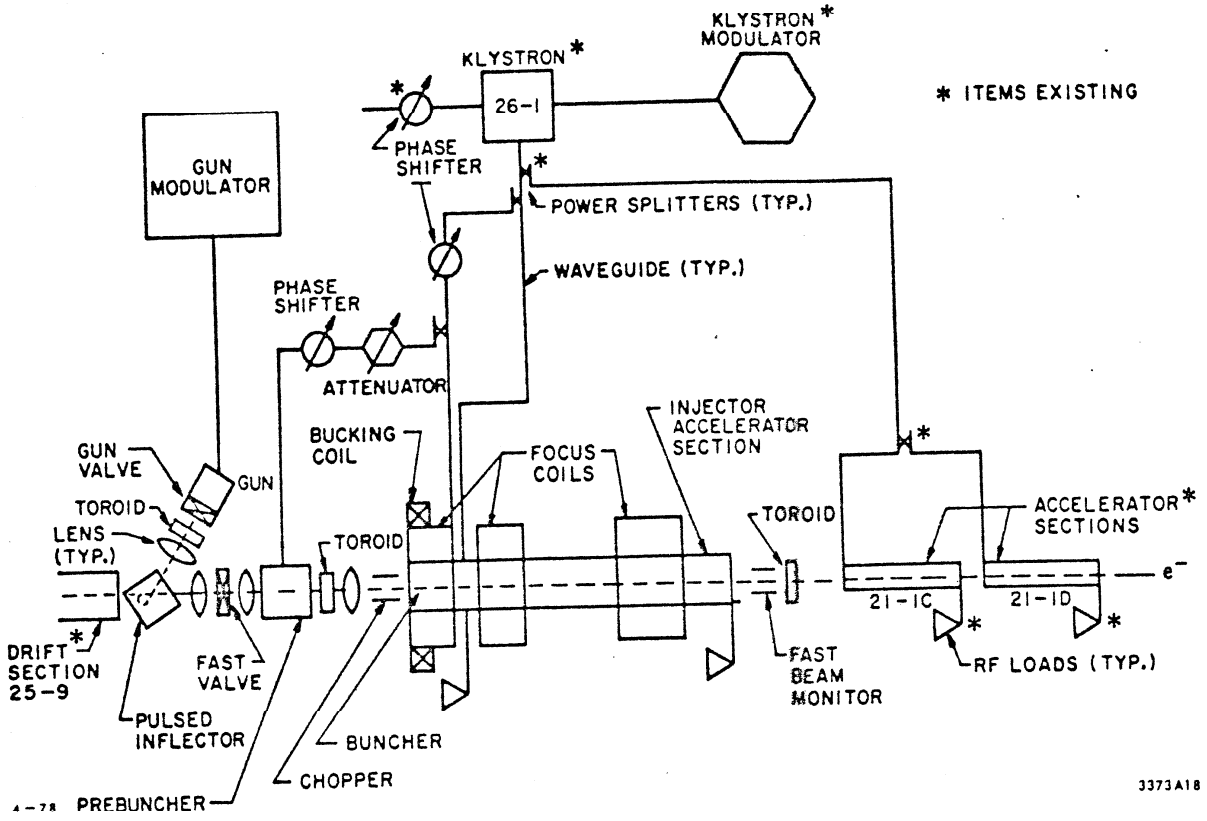

Fig. A.1. Schematic of the proposed Injector East

electrons enter the new injector through a pulsed inflector magnet. The entire device can be switched on or off on a pulse-to-pulse basis, and operated either by itself or interleaved with other full energy beams. The energy, intensity and quality of the new beam will be determined by the performance of the new injector and the last five sectors of the machine. With an energy gain of 700 MeV per sector, the five-sector beam will have a maximum energy

of 3.5 GeV unloaded. The maximum beam current determined by BBU threshold will be much higher than for a comparable beam in the full machine because the beam does not have to pass through so many unused sections which contribute to beam breakup.

To get a realistic idea of the maximum currents we might expect under real operating conditions, some measurements of BBU threshold were taken using the first five sectors of the SLAC linac with focusing adjusted to simulate the conditions in the last five sectors (G. A. Loew and R. Miller, unpublished internal SLAC report). The results of these measurements are shown in Fig. A.2. There we see, for example, that for a beam with one sector of acceleration up to 0.4 GeV and then coasting through four sectors,

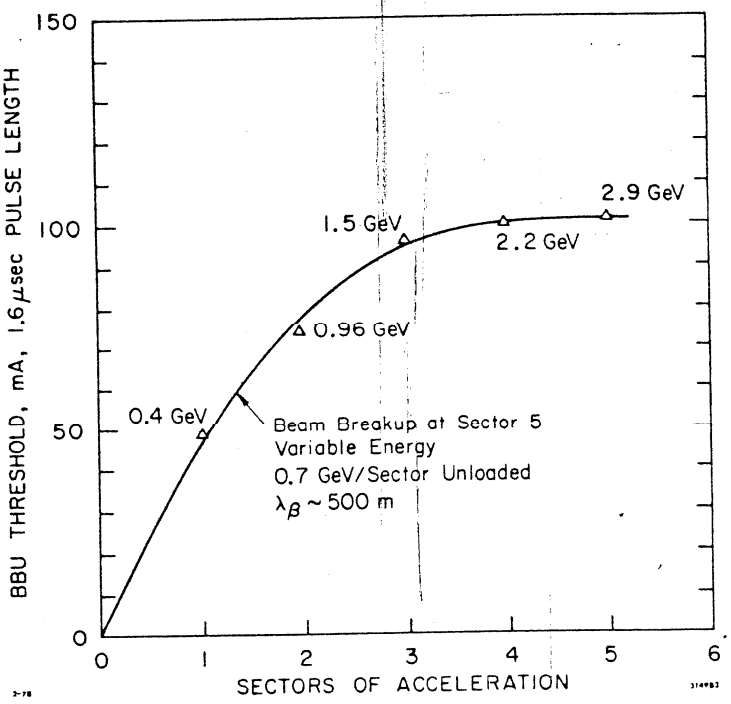

Fig. A.2. Experimental measurements of Beam Breakup Threshold at the end of Sector 5 for fixed betatron wavelength $\lambda_\beta \sim 500$ m (easily available now in Sectors 26-30) and variable energy obtained by accelerating beam up to sector shown and then letting it coast.

the maximum current at the end of Sector 5 is 50 mA peak for a 1.6 usec pulse length. With five sectors of acceleration the maximum current is 100 mA peak and the loaded beam energy is 2.9 GeV. This performance curve indicates that the new injector would

produce a beam with intensity 50 to 100 times that now presently available at SLAC in the energy range 0.4 to 2.9 GeV. We expect the beam quality (energy spread and angular emittance) to be roughly similar to the present high energy SLAC beams, i.e., 80% transmission through $\pm$ 0.2% slits.

Technically the new injector is a straightforward simplified replica of the existing injector with no new problems. Its performance and cost do not depend on any new developments in technology. A complete breakdown of the cost estimate has been prepared by the SLAC staff and is included below.

In order to fine tune the energy of the five-sector beam, it is necessary to provide separate trigger pulses and phasing control to individual klystrons in one sector rather than for a whole sector at a time as is presently done. For that purpose provision is made for new instrumentation listed under the heading "Beam Loading Sector Trigger Generator" in the enclosed estimate.

APPENDIX B

MONOCHROMAT

In this appendix we describe a possible future development, called the Monochromat, not proposed at this time, to improve the energy spectrum of the SLAC linear accelerator by a factor of 10 to 30 with no loss in beam intensity. This would be accomplished by installing a radio-frequency separator in the A-line downstream from the high power slits, as shown in Fig. B.1. This scheme was suggested by R. Miller of SLAC and has been described in more detail in Ref. (K6). The rf separator sections can be phased so that the center phase of the electron bunch is at the point in time when the transverse electric and magnetic fields vanish and the longitudinal electric fields, which are zero on the axis and vary linearly in the horizontal coordinate x, are maximum. The electron beam, dispersed horizontally at the separator with horizontal position correlated with momentum, is then compressed in momentum.

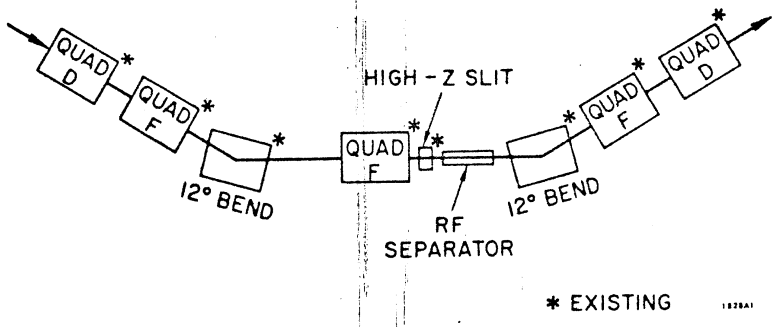

Fig. B.1. Schematic of an energy compression system for the SLAC A-line.

The shunt impedance of the separators built at SLAC is

$$r_x = \frac{\left[\frac{\lambda}{2\pi}\frac{\partial E_z}{\partial x}\right]}{-\frac{dp}{dz}} = 16\ \text{M}\Omega/\text{meter}$$

where E_z is the axial electric field and p is the power flow in the structure. The dispersion of a 20 GeV beam at the separator would be 27.5 MeV/cm. With two 6-meter separator structures connected in tamdem and driven by a single klystron, the attenuation per section would be -0.8 nepers and the power required would be 14.5 MW. The aperture of the separator is about 4.5 cm which corresponds to an energy acceptance of 0.6%.

An important consequence of adding the rf separator is that the horizontal emittance of the beam is greatly increased. The monochromat rotates the beam in the $x\text{-}p_z$ phase plane; thus, if the bunch is a δ-function in z, the transverse horizontal emittance increases by the same factor that the energy spread is reduced. The rf separator also shears the beam in the $z\text{-}p_z$ phase plane and thus further increases the transverse horizontal emittance by a factor of 3 to 5. Typically, the horizontal emittance increases by a factor of about 100 to $2\pi \times 10^{-4}$ cm-rad. The table below shows the computed rms extent of the beam in each of the six dimensions of phase space at the input and output of the Monochromat with the 12 meter long separator structure represented as four lumped elements spaced 3 meters apart:

Table A

	Input		Output	
x(cm	0.100	waist	0.525	waist
θ(mrad)	0.020		0.514	
y(cm)	0.200		0.177	
ϕ(mrad)	0.020		0.023	
z(bunch length)(cm)	0.100		0.384	
$\delta p_z/p_z$ (%)	0.200		0.006	

The overall resolution depends on a number of factors: magnetic field uniformity and stability of the analyzing magnets; error in beam positioning in the separator; the shearing effect which depends on field strengths, bunch length and separator length; and beam collimation at the input. R. Miller estimates that the overall practical resolution is limited by these factors to about 0.01%.

The cost of the device would depend upon the length of the rf separator desired. In Ref. (K6) R. Miller describes a configuration using a 12 m section powered by 1 klystron which would work for beam energies up to 20 GeV. At our request the SLAC staff has prepared a complete cost estimate for a Monochromat using one existing 10-foot separator section and one klystron which would be adequate for beam energies up to about 5 GeV. The total cost, including indirect charges, the DOE added factor, and 20% contingency, is $394,181 at FY1979 rates.

REFERENCES

A. Experiment, Our Previous Experiments

A1. R. G. Arnold, et al., Phys. Rev. Lett. 35, 776 (1975).

A2. W. P. Schutz, et al., Phys. Rev. Lett. 38, 259 (1977).

A3. F. Martin, et al., Phys. Rev. Lett. 38, 1320 (1977).

A4. R. G. Arnold, et al., SLAC-Pub-2093, Phys. Rev. Lett. 40, 1429 (1978).

A5. S. Rock, et al., contributed paper to the 1977 International Symposium on Lepton and Photon Interactions at High Energies, Hamburg, Germany (1977), and abstract submitted to the APS meeting, Washington, D.C., April 23-27 (1978).

A6. SLAC Experiment E133, "Measurement of Elastic Electron-Neutron Cross Section at High Q^2," approved Feb. 1978, beam time not yet scheduled.

B. Experiment, e-d Elastic and Threshold Electrodisintegration

B1. B. Grossetete, et al., Phys. Rev. 141, 1425 (1966).

B2. D. Benaksas, et al., Phys. Rev. Lett. 13, 353 (1964).

B3. D. Ganichot, et al., Nucl. Phys. A178, 545 (1972).

B4. C. Buchanan and M. Yearian, Phys. Rev. Lett. 15, 303 (1965).

B5. R. Rand, et al., Phys. Rev. Lett. 18, 469 (1967), R. Rand, et al., Phys. Rev. D8, 3229 (1973).

B6. W. Atwood, Thesis SLAC Report 185 (1975).

B7. G. Simon, et al., Phys. Rev. Lett. 37, 739 (1976).

B8. E. M. Riordan, et al., SLAC-Pub-1634 (1975)

B9. J. S. Poucher et al., Phys. Rev. Lett. 32, 118 (1974).

B10. M. R. Yearian, E. B. Hughes, Phys. Lett. 10, 234 (1964)

B11. H. W. Kendal, et al., Phys. Rev. 124, 1596 (1961).

C. Experiment, e-^{3}He and e-^{3}H

C1. J. S. McCarthy, et al., Phys. Rev. C15, 1396 (1977) and references therein for low q data.

C2. M. Bernheim, et al., Lett. Nuovo Cim 5, 431 (1972).

C3. H. Collard, et al., Phys. Rev. B138, 57 (1965).

D. e-d Elastic, Nonrelativistic Nuclear Theory

D1. A. D. Jackson, A. Lande, D. Riska, Phys. Lett. 55B, 23 (1975).

D2. M. Gari and G. Hyuga, Nucl. Phys. A264, 409 (1976), Phys. Rev. Lett. 36, 345 (1976), Nucl. Phys. A278, 372 (1977).

D3. M. Gari, H. Hyuga, B. Sommer, Phys. Rev. C14, 2196 (1976).

D4. W. Fabian and H. Arenhovel, Phys. Rev. Lett. 37, 550 (1976).

E. e-d Elastic, Relativistic Theory

E1. R. G. Arnold, C. Carlson, F. Gross, Phys. Rev. Lett. 38, 1516 (1977).

E2. F. L. Ridener, Jr., H. S. Song, R. H. Good, Jr., Penn. State University Preprint (1978).

E3. A. Fernandez-Pacheco, J. A. Grifols, I. Schmidt, SLAC-Pub-2088.

E4. F. Gross, Invited Paper, Proceedings VIIth International Conference on High Energy Physics and Nucl. Structure, Zurich, Switzerland (1977), p. 329.

E5. F. Gross, Invited Paper, VIIth International Conference on Few Body Problems in Nuclear and Particle Physics, Delhi, India (1976), (edited by Mitra, et al., North Holland Pub. Co.) p. 523.

E6. W. W. Buck and F. Gross, Phys. Lett. 63B, 286 (1976), and F. Gross, private communication.

E7. F. Gross, Invited Paper submitted to International Conference on Few Body Problems in Nuclear Physics, Graz, Austria, 24-30 Aug., 1978.

F. Nonrelativistic Nucleon-Nucleon Potential Models

F1. M. J. Moravcsik, P. Ghosh, Phys. Rev. Lett. 32, 321 (1974). This paper contains a description of the world's supply of deuteron models up to 1974.

F2. R. V. Reid, Ans. Phys. (NY) 50, 411 (1968).

F3. K. Holinde, R. Machleidt, Nucl. Phys. A247, 495 (1975).

F4. K. Holinde, R. Machleidt, Nucl. Phys. A256, 479 (1976), Nucl. Phys. A256, 497 (1976)

F5. The HM1, HM2, and HM3 wave functions used here were obtained from polynomial fits by F. Gross, private communication.

G. Deuteron Electrodisintegration, Nuclear Theory

G1. V. Z. Jankus, Phys. Rev. 102, 1586 (1956).

G2. R. J. Adler, Phys. Rev. 169, 1192 (1968).

G3. D. O. Riska, Invited Paper, Proceedings International Conference on Photonuclear Reactions and Applications, Asilomar (1973) p. 337.

G4. J. Hockert, et al., Nucl. Phys. A217, 14 (1973).

G5. J. A. Lock and I. L. Foldy, Phys. Lett. 51B, Ans. Phys. 93, 276 (1975).

G6. B. Mosconi and P. Ricci, Nuovo Cim A23, 401 (1974).

G7. W. Fabian and H. Arenhovel, Nucl. Phys. A258, 461 (1976).

G8. Results from Fabian and Arenhovel, Nucl. Phys. A258, 461 (1976) extended to larger Q^2 were provided by H. Arenhovel, private communication.

G9. D. O. Riska and G. E. Brown, Phys. Lett. 38B, 193 (1972).

G10. B. Sommer, Deuteron Electrodisintegration at High Energy and Momentum Transfer, preprint, Institute fur Theoretische Physik, Ruhr-Universitat Bochum, Germany (1978).

H. Deuteron and Proton Electrodisintegration, High Energy Theory

H1. S. D. Drell, T. M. Yan, Phys. Rev. Lett. 24, 181 (1970)

H2. G. B. West, Phys. Rev. Lett. 24, 1206 (1970).

H3. E. Bloom and F. Gilman, Phys. Rev. D4, 2901 (1971).

H4. G. Farrar and D. Jackson, Phys. Rev. Lett. 35, 1416 (1975).

H5. L. Frankfurt and M. I. Strikman, Phys. Lett. 65B, 51 (1976).

H6. G. West, Phys. Rev. Lett. 37, 1454 (1977).

H7. G. West, Phys. Rev. D14, 732 (1976)

I. ^{3}He and ^{3}H, Nuclear Theory

I1. A. D. Jackson, et al., Nucl. Phys. A156, 1 (1970)

I2. L. M Delves, M. A. Hennell, Nucl. Phys. A168, 347 (1971), A246, 490 (1975).

I3. M. R. Strayer, P. U. Sauer, Nucl. Phys. A231, 1 (1974).

I4. R. A. Brandenburg, et al., Phys. Rev. C12, 1368 (1975), A. E. L. Dieperink, et al., Phys. Lett. 63B, 261 (1976).

I5. A. Laverne, C. Gignoux, Phys. Rev. Lett. 29, 436 (1973).

I6. W. M. Kloet, J. A. Tjon, Phys. Lett. 49B, 419 (1974), Phys. Lett. 61B, 356 (1976).

I7. R. A. Brandenburg, Y. E. Kim, A. Tubis, Phys. Rev. Lett. 32, 1325 (1974).

I8. R. A. Brandenburg, P. U. Sauer, Phys. Rev. C12, 1101 (1975).

I9. A. Barroso and E. Hadjimichael, Phys. Lett. 47B, 103 (1973), Nucl. Phys. A238, 422 (1975).

I10. E. Hadjimichael, Phys. Lett. 63B, 161 (1976).

I11. E. Hadjimichael, Nucl. Phys. A294, 513 (1978).

I12. M. I. Haftel, W. M. Kloet, Phys. Rev. C15, 404 (1977).

I13. J. Borysowicz, D. O. Riska, Nucl. Phys. A254, 301 (1975), and Michigan State University internal report (1978).

J. Quarks in Nuclear Physics

J1. S. Brodsky and G. Farrar, Phys. Rev. D11, 1309 (1975).

J2. The CIM model has been developed in a series of papers by S. Brodsky, R. Blankenbecler, J. Gunion and others. A recent review of the high transverse momentum phenomena including a description of the CIM is given in D. Sivers, S. J. Brodsky, R. Blankenbecler, Phys. Rep. 23C, No. 1 (1976).

J3. S. Brodsky and B. Chertok, Phys. Rev. D14, 3003 (1976), Phys. Rev. Lett. 37, 269 (1976).

J4. I. Schmidt and R. Blankenbecler, Phys. Rev. D15, 3321 (1977), SLAC-Pub-1931 (1977)

J5. I. Schmidt, Thesis SLAC Report 203 (1977).

J6. V. Matveev and P. Sorba, Fermilab Pub. 77/36 THY (1977).

J7. V. Matveev and P. Sorba, Lett. Nuovo Cim 20, 435 (1977).

J8. A. P. Kobushkin ITP-77-113E, Kiev, USSR (1977).

J9. A. Vainshtein and V. Zakharov, Phys. Lett. 72B, 368 (1978).

J10. C. DeTar, Phys. Rev. D17, 302 (1978) and D17, 323 (1978).

J11. B. T. Chertok, Submitted to Phys. Rev. Lett.

J12. C. G. Callan, D. J. Gross, Phys. Rev. Lett. 22, 156 (1969)

K. General

K1. Facilities for 180° electron scattering at lower energies have been developed at IKO in Amsterdam and at the Bates Linac at MIT.

K2. T. de Forest, Jr., and J. D. Walecka, Advances in Physics 15, 1 (1966).

K3. R. Beurtey, Isobars in Nuclei, Invited Paper, Proceedings International Conference on High Energy Physics and Nuclear Structure, Santa Fe, N.M. (1975), p. 653.

K4. Workshop on Recent Developments Involving Isobars in Nuclear Systems, Proceedings VIIth International Conference on High Energy Physics and Nuclear Structure, Zurich, Switzerland (1977), p. 193.

K5. The Role of Electron Accelerators in U.S. Medium Energy Nuclear Science, DOE/NSF Report ORNL/PPA-77/4, R. S. Livingston, Chairman (1977).

K6. R. H. Miller, et al., IEEE Vol. NS 18, 604 (1971) and internal SLAC Memo by R. H. Miller, "Conversion of A-line to High Energy Resolution (0.01%) High Current (30 mA) Beam Line," 19 Feb. 1971.

L. Experiment - Quasi Elastic Scattering

L1. J. R. Dunning, et al., Phys. Rev. 141, 1286 (1966)

L2. R. J. Budnitz, et al., Phys. Rev. 173, 1357 (1968)

L3. K. M. Hanson, et al., Phys. Rev. D8, 753 (1973)

L4. W. Bartel, et al., Nucl. Phys. B58, 429 (1973)

L5. J. S. McCarthy, et al., Phys. Rev. C13, 712 (1976)

L6. A. E. L. Dieperink, et al., Phys. Lett. 63B, 261 (1976)